

Energy & Environmental Science

Accepted Manuscript



This is an *Accepted Manuscript*, which has been through the Royal Society of Chemistry peer review process and has been accepted for publication.

Accepted Manuscripts are published online shortly after acceptance, before technical editing, formatting and proof reading. Using this free service, authors can make their results available to the community, in citable form, before we publish the edited article. We will replace this *Accepted Manuscript* with the edited and formatted *Advance Article* as soon as it is available.

You can find more information about *Accepted Manuscripts* in the [Information for Authors](#).

Please note that technical editing may introduce minor changes to the text and/or graphics, which may alter content. The journal's standard [Terms & Conditions](#) and the [Ethical guidelines](#) still apply. In no event shall the Royal Society of Chemistry be held responsible for any errors or omissions in this *Accepted Manuscript* or any consequences arising from the use of any information it contains.

Combining experimental and theoretical methods to learn about the reactivity of gas-processing metalloenzymes[†]

Claudio Greco^c, Vincent Fourmond,^a Carole Baffert,^a Po-Hung Wang,^{d,e} Sébastien Dementin,^a Patrick Bertrand,^a Maurizio Bruschi,^c Jochen Blumberger,^{*d} Luca de Gioia,^{*b} Christophe Léger^{*a}

Last edited September 7, 2014, Received Xth X 20XX, Accepted Xth X 20XX

First published on the web Xth X 20XX

DOI: 10.1039/000000

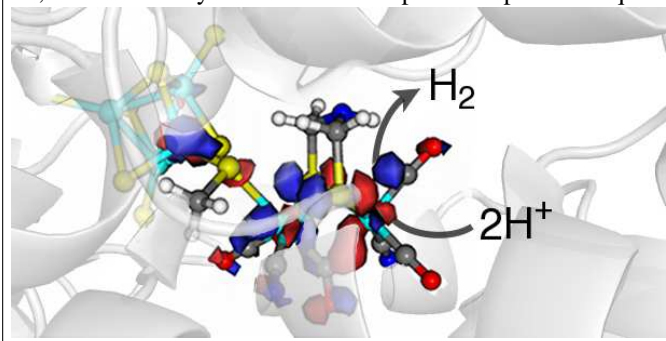
1 After enzymes were first discovered in the late XIX cen-
2 tury, and for the first seventy years of enzymology, kinetic
3 experiments were the only source of information about en-
4 zyme mechanisms. Over the following fifty years, these
5 studies were taken over by approaches that give informa-
6 tion at the molecular level, such as crystallography, spec-
7 troscopy and theoretical chemistry (as emphasized by the
8 Nobel Prize in Chemistry awarded last year to M. Karplus,
9 M. Levitt and A. Warshel). In this review, we thoroughly
10 discuss the interplay between the information obtained
11 from theoretical and experimental methods, by focussing
12 on enzymes that process small molecules such as H₂ or
13 CO₂ (hydrogenases, CO-dehydrogenase and carbonic an-
14 hydrase), and that are therefore relevant in the context of
15 energy and environment. We argue that combining theo-
16 retical chemistry (DFT, MD, QM/MM) and detailed inves-
17 tigations that make use of modern kinetic methods, such
18 as protein film voltammetry, is an innovative way of learn-
19 ing about individual steps and/or complex reactions that
20 are part of the catalytic cycles. We illustrate this with re-
21 cent results from our labs and others, including studies of
22 gas transport along substrate channels, long range proton
23 transfer, and mechanisms of catalysis, inhibition or inacti-
24 vation.

1 Introduction

27 Chemists are fascinated by the catalytic power of enzymes,
28 which accelerate reactions by many orders of magnitude.
29 Since they were discovered, more than a century ago, the

Broader context:

Some reactions which are very important in the context of energy and environment, such as the conversion between CO and CO₂, or H⁺ and H₂, are catalyzed in living organisms by large and complex enzymes that use inorganic active sites to transform substrates, chains of redox centers to transfer electrons, ionizable amino acids to transfer protons, and networks of hydrophobic cavities to guide the diffusion of substrates and products within the protein. This highly sophisticated biological plumbing and wiring makes turnover frequencies of thousands of substrate molecules per second possible. Understanding the molecular details of catalysis is still a challenge. We explain in this review how a great deal of information can be obtained using an interdisciplinary approach that combines state-of-the-art kinetics and computational chemistry. This differs from — and complements — the more traditional strategies that consist in trying to *see* the catalytic intermediates using methods that rely on the interaction between light and matter, such as X-ray diffraction and spectroscopic techniques.



amount of information that has been acquired about their working principles has been phenomenal. Thanks to the contributions of many physical chemists, great progress has been made regarding the use of both classical and quantum mechanics to describe the mechanism at a molecular level. However, depending on the intrinsic complexity of the catalytic system, the level of understanding that theoretical chemists can achieve varies greatly.

^a Aix Marseille Université, CNRS, BIP UMR 7281, 13402, Marseille, France. Tel: +33 4 91 16 45 29; E-mail: christophe.leger@imm.cnrs.fr

^b Università di Milano Bicocca, Department of Biotechnology and Biosciences, Piazza della Scienza 2, 2016, Milan, Italy; E-mail: luca.degioia@unimib.it

^c Università di Milano Bicocca, Department of Earth and Environmental Sciences, Piazza della Scienza 1, 2016, Milan, Italy

^d University College London, Department of Physics and Astronomy, London WC1E 6BT, UK. E-mail: j.blumberger@ucl.ac.uk

^e Po-hung Wang's present address: Theoretical Molecular Science Laboratory, RIKEN 2-1 Hirosawa, Wako-shi, Saitama, 351-0198, Japan

Regarding enzymes that have either no cofactors or organic cofactors, and where the chemical transformation of the substrate occurs at the protein surface, substrate binding is essentially a matter of docking (rather than a complicated, intramolecular, multi-step diffusive process) and the main features of the mechanism can be inferred from X-ray data and site-directed mutagenesis experiments that identify the crucial amino acids. In these cases, theoretical chemists can focus on detailed yet important aspects of function, such as the role of protein motions in determining the turnover rate. Complications may arise in the case of “floppy” enzymes where a large conformational change on the micro-second time scale might partly determine the turnover rate.

The situation is very different in the case of many other enzymes (including some of those discussed here) that use an inorganic cofactor to transform a small substrate. This is for several reasons: (1) X-ray investigations often give an ambiguous picture of the structure of the active site, and/or, as occurs with hydrogenases, cannot detect the substrate because it is not sufficiently electron-dense; (2) The reactivity of complex inorganic active sites is sometimes difficult to predict, in part because it is largely tuned by the surrounding protein matrix, so that the catalytic mechanism is far from being straightforward (the exact mode of substrate binding, the sequence of events that take place at the active site during catalysis are often unknown); (3) Theoretical methods have not yet been tuned to achieve the same accuracy as with organic cofactors, so that the results of calculations must be considered with caution; (4) These enzymes often house several cofactors and the catalytic mechanism involves a number of steps which are very different in nature (long range intramolecular substrate and product diffusion, long range proton and electron transfers and active-site chemistry *per se*) which occur on sites of the protein that are very far apart from one another. Any of these steps may, under certain conditions, limit the overall rate of the reaction and therefore determine the enzyme’s global catalytic properties. Often it cannot even be ascertained that active site chemistry limits the rate of turnover and regarding three out of the four enzymes discussed here, the calculation of turnover rates using theoretical methods still appears to be out of reach. A combination of theoretical chemistry and experimental methods can nonetheless be very useful to understand many different aspects of the mechanism, as discussed herein.

Figure 1 summarizes the different approaches, both experimental and theoretical, that can be used independently or in combination to find out how such complex catalysts work. The outcome of experiments and calculations are the observables listed in the central column of fig. 1 and organized in three groups: thermodynamic, structural and kinetic properties. The mechanism itself is not an observable, which is the main reason why theoretical calculations are essential. Of course, experimental observables derive from the structure and reactivity

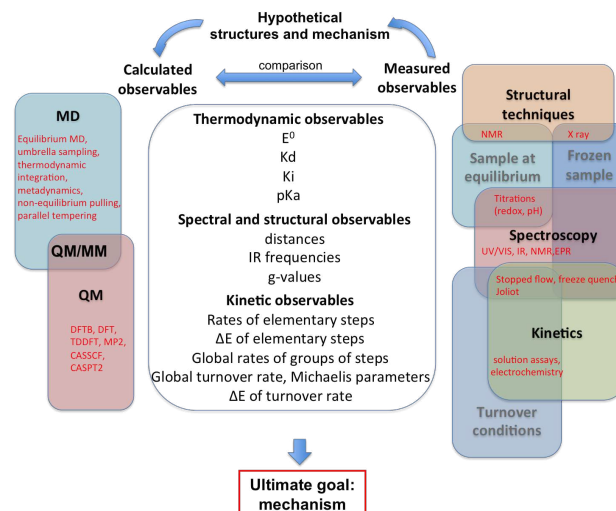


Fig. 1 This figure shows a list of the observables that can be calculated or experimentally measured, and the feedback process that can lead to understanding a catalytic mechanism.

of the enzyme, but in such a complex way that it is generally not possible to deduce the mechanism from the values of the observables. In that respect, confronting theoretical results to experimental observations can help uncover the molecular details of the catalytic mechanism of an enzyme. This process is sketched in fig. 1 and illustrated in the last section of this paper.

The feedback process shown on top of fig. 1, which is the key to understand the mechanism, is necessarily bootstrapped by experimental observations. We have classified the latter into three main approaches (structural, spectroscopic, kinetic), which can be used to probe three kinds of enzyme samples (at equilibrium, frozen, or turning over under catalytic conditions). Our goal here was not to list all existing techniques, but to show how they relate to each other. Any experiment, indicated in red in the right part of scheme 1, is at the intersection between two or several domains: for example a redox titration consists in using a spectroscopic technique to monitor the redox state of a sample under equilibrium conditions. Experimental observables are very complex functions of the structures and kinetic properties of intermediates of the catalytic cycle. They can be interpreted to give structural or mechanistic information (e.g. “this IR spectrum shows that there are probably 3 CO ligands”, or “the pH dependence of this rate constant shows that the corresponding reaction involves a protonation”), but they do not usually give a complete description of the catalytic mechanism.

As illustrated in section 4, direct electrochemistry has proved important in kinetic investigations of metalloenzymes,¹ and we briefly introduce the technique here. En-

zyme molecules are adsorbed or covalently attached^{2,3} as a submonolayer onto an electrode; the electrode potential is set to a value that forces the oxidation or the reduction of the enzyme, and the continuous catalytic transformation of substrate results in a flow of electrons across the electrode. This catalytic current is proportional to the turnover frequency times the electroactive coverage of enzyme participating in the reaction. If the electroactive coverage is constant, the current is proportional to turnover rate. That the current can be sampled at sub-second intervals is a strong advantage compared to traditional solution assays. Most significantly, using an electrode adds a control parameter (the electrode potential) to traditional enzyme kinetic measurements performed in solution. By changing the electrode potential, using steps or sweeps, it is possible to observe how the enzyme responds to changes in driving force. Provided that kinetic models are used to quantitatively interpret the data, information can be gained about the properties of the enzyme's redox centers and the kinetics of intramolecular electron transfer^{4,5}, or the (in)activation of the enzyme that often occurs under conditions of extreme potential⁶⁻⁸. The concentrations of substrate, product or inhibitors can also be changed while the activity is being recorded, making it easy to determine Michaelis and inhibition constants but also, and most importantly, rates of the reaction with inhibitors^{9,10}. The technique has obvious limitations: not all enzymes can be directly wired to electrodes and some artefacts sometimes arise from the protein/electrode interaction. We have discussed in a previous review some of the artifacts that may occur in PFV experiments¹. Apart from that, the main pitfalls of the technique are the same as those described in all enzyme kinetics textbooks: observing an agreement between a kinetic model and experimental data does not imply that the model is correct (or unique), and ingenious approaches have to be used to learn about the rates of individual steps in the catalytic cycle, or the molecular mechanisms of the chemical transformations that are at stake, based on a *global* measurement of turnover rate.

Regarding mechanistic investigations, it is important to realize that key intermediates are intrinsically short-lived, and consequently difficult to accumulate, detect and characterize experimentally. This implies that experimental results often need to be complemented by theoretical studies. The growing role of quantum chemical methods in the investigation of metalloenzymes is well testified by the Nobel Prize in Chemistry 2013, which was awarded to Martin Karplus, Michael Levitt and Arieh Warshel for the development of multiscale computational models of complex chemical systems, i.e. the development of methods, based on classical and quantum mechanical theory, which can be used to study large chemical systems and their reactivity.

The computational methods used to study the molecular properties of metalloenzymes can be classified into two fam-

ilies (left part of fig. 1). The first includes methods grounded in classical physics, such as Molecular Mechanics (MM) and Molecular Dynamics (MD). MM methods are used to calculate potential energies, whereas the goal of MD calculations is to describe the evolution of the structure of the protein, using Newton equations, based on the known energies of interaction between different atoms. MM and MD calculations allow to investigate the "physical" properties of the system, such as the dynamics of proteins in solution, as well as the diffusion of substrates and inhibitors into enzymes, but such approaches cannot be used to investigate properties that explicitly depend on electrons, such as reaction pathways and most spectroscopic features. The second family of computational tools includes Quantum Mechanical (QM) methods, which allow to calculate reaction energies and spectroscopic properties. QM methods are now routinely used to investigate large molecular systems, such as the active site of enzymes. Among all available QM methods, those based on the Density Functional Theory (DFT) are extremely popular due to their favorable trade-off between accuracy and computational costs.

In the context of bioinorganic chemistry, theoretical methods are useful for learning about active site geometries, for interpreting spectroscopic properties, and for elucidating reaction mechanisms (based on the energies of minima and saddle points along putative reaction pathways). The calculated observables are the same as those determined from experiments, but the approach usually takes a different route. In most theoretical calculations, especially QM, one needs to first postulate a structure or mechanism and then compute the observables. That the calculated observables match the measured ones suggests that the postulated structures are correct. Or the fact that calculated observables do not match experimental ones demonstrates that the mechanistic hypotheses can be ruled out. The comparison with experimental results is also fundamental to ensure that the system is described with sufficient accuracy with the approximations used (for instance, in quantum chemical calculations one has to choose the level of theory, the basis set, the cluster size, etc.). Comparison between theory and experiments can be made on different levels, from a qualitative point of view ("this intermediate is much too high in energy, so it is very unlikely that catalysis proceeds this way") to semi-quantitative ("theory predicts that this species should be easier to oxidize than this one, in agreement with the experiments") or quantitative (comparing the calculated and measured values for IR frequencies or rate constants).

Recently, advances in both experimental and theoretical methods have favored the dialogue between the "wet lab" and *in silico* approaches, and this interaction can now provide answers to open issues in the field of enzyme-catalyzed fuel production. In the present paper, we aim at showing how the combination of computational and experimental methodolo-

gies in enzymological studies can be fundamental for favoring the cross-fertilization of ideas, which is a prerequisite for any future change of paradigm in energy production and supply.

In fact, since most technological processes currently rely directly or indirectly on fossil fuels, which are non-renewable (in non-geological time scales) and consumed at an ever-increasing rate, one challenge facing current world economy is related to the availability and cost of energy. In addition, the burning of fossil fuels is continuously increasing CO₂ concentration in the atmosphere, causing environmental problems. Therefore, the development and exploitation of alternative and renewable fuel sources and energy carriers, as well as advances in CO₂ processing technologies, have very high priority.

The production of solar fuels is one of the best answers to such energy and environmental crisis and certainly one of the grand challenges of this century. Storing sunlight in the form of energy-rich chemical bonds offers the prospect of using existing or only slightly modified technologies that currently run on fossil fuels, such as e.g. car engines. Biology provides much inspiration for the development of such catalysts. Over millions of years, Nature has evolved highly efficient metal-clusters bound to proteins, for the purpose of converting small, inert molecules such as CO₂, N₂ and even water, with the help of sunlight, into highly energetic molecules (fuels) such as CO, methanol, ammonia or H₂. We believe that a deep understanding of these fundamental biological reactions will provide the key for a successful translation into artificial processes. For this to happen, it will be vital to take advantage of the synergistic strengths of combined experimental and computational approaches.

Here is the structure of the paper and the scope of each section. In the second section of this paper, we introduce and describe the structures of the four enzymes that we shall discuss throughout the paper. In the third section we discuss how observables can be either measured in experiments or calculated, and at which accuracy; we shall also illustrate the drawbacks and pitfalls of several approaches. In the last section of this paper, we critically discuss selected literature in this field. We identify certain discrepancies between experimental and theoretical results, and gaps in the existing knowledge that will clearly be of interest in the future. We emphasize cases where combining experiments and theory provided much more insights than using the two approaches independently. Theoreticians should be able to start from educated guesses based on the experimentalists' results, while experimentalists should be able to perform the experiments that help discriminate between different hypotheses. This synergy is illustrated with several examples taken from our work and the work of others, focussing on four different metalloenzymes, three oxidoreductases ([NiFe] and [FeFe]-hydrogenases, carbon monoxide dehydrogenase) and one non-redox enzyme (carbonic anhy-

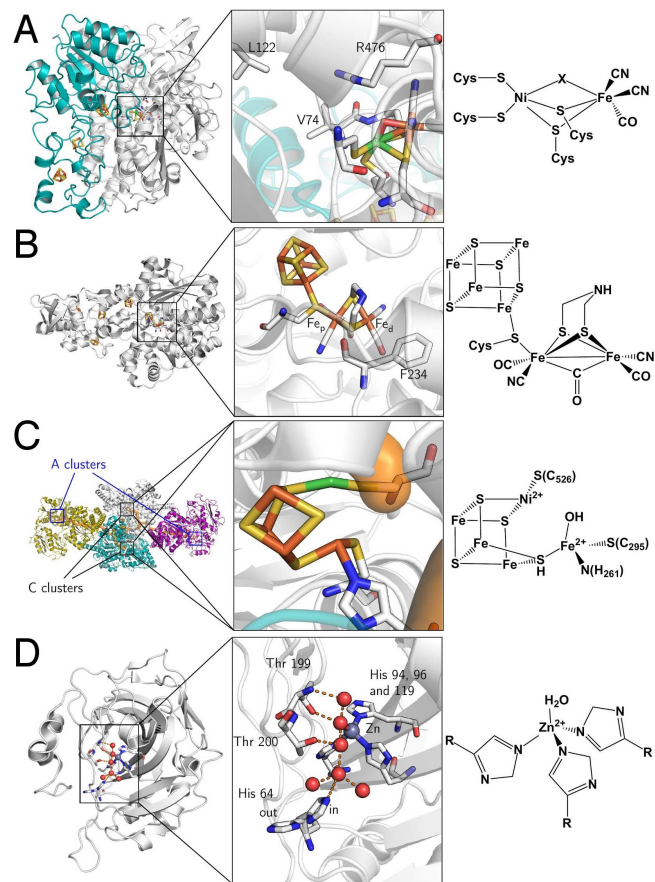


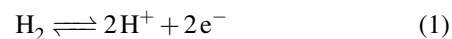
Fig. 2 Protein structures and active site structures of the four enzymes discussed in the last section of this paper: [NiFe]-hydrogenase (A), [FeFe]-hydrogenase (B), Acetyl-CoA synthase / CO-dehydrogenase (C) and carbonic anhydrase (D). The structures were drawn respectively from PDB 1YQW, 3C8Y, 2Z8Y and 3KS3.

drase), all of which catalyse reactions of importance in the context of renewable energy and environmental-friendly processes.

2 Background information about the four enzymes discussed in this paper

2.1 Hydrogenases

Hydrogenases^{11,12} are enzymes that catalyse the reversible oxidation of H₂ into protons and electrons according to:



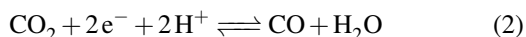
They are divided into two classes based on the metal content of their active site. The so-called “[NiFe]-hydrogenases” house a dinuclear [NiFe] active site, in which the Ni is coordinated by

4 cysteines (two of which bridge the metal ions), and the Fe is coordinated by two CO and one CN⁻ ligand (fig. 2A). MD and DFT calculations suggest that H₂ binds to the Ni ion^{13,14}. The active site is buried inside the protein matrix, and connected to the solvent *via* a hydrophobic tunnel that guides the transport of substrate, a network of protonatable amino acids that transfer protons to/from the active site, and a chain of three iron-sulfur clusters to mediate electron transfer to/from the redox partner. These clusters are referred to as “proximal”, “medial” and “distal” according to their distance from the active site.

[FeFe]-hydrogenases oxidize or produce H₂ at an active site, the so-called H cluster, that is composed of a standard [4Fe4S] cluster covalently attached by a cysteine residue to a [Fe₂(CO)₃(CN)₂(dtma)] subsite (dtma = dithiomethylamine)^{15,16} (fig. 2B). The iron atoms of this [FeFe] subsite are named proximal (Fe_p) or distal (Fe_d) according to the distance to the [4Fe4S] cluster. In the catalytic mechanism, the [FeFe] subsite cycles between at least two redox states, referred to as Hox and Hred, which can be formally described as Fe(II)Fe(I) and Fe(I)Fe(I), respectively. Dihydrogen or protons (depending on the direction of the reaction) bind on the distal Fe. The enzyme from *Chlamydomonas reinhardtii* (Cr) has no cofactor other than the H cluster. The enzymes from *Clostridium pasterianum* (Cp) and *Clostridium acetobutylicum* (Ca) bind 4 additional FeS clusters, which act as electron relays. The enzyme from *Desulfovibrio desulfuricans* (Dd) houses the H cluster and two [4Fe4S] clusters.

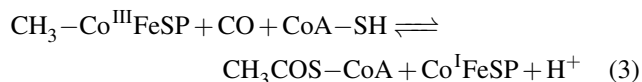
2.2 ACS/CODH

Acetyl-CoA synthase / CO-dehydrogenase (ACS/CODH) is a bifunctional enzyme that plays a crucial role in anaerobic bacteria such as acetogenic organisms, which rely on the Wood-Ljungdahl pathway of carbon fixation¹⁷. It is estimated that ≈ 10¹¹ tons of acetate per year are produced globally from CO₂ through this pathway¹⁸. ACS/CODH catalyses the synthesis of acetyl-CoA from CO₂, CoA, and a methyl group donated from the corrinoid-iron-sulfur protein (CoFeSP). This complex reaction occurs in two steps, that take place in different subunits: the two-electron reduction of CO₂ to CO according to reaction 2 is catalysed in the β subunit, at the C cluster, a [NiFe₄S₄] active site (fig. 2C).



It is proposed that CO₂ binds the C cluster in the so-called C_{red2} redox state, with the C atom of CO₂ bound to Ni(0), and the O atom to a Fe(II) atom of the cluster. CO and water release leaves the cluster in the C_{red1} state (Ni(II)Fe(II)). Electrons are transferred via the B and D clusters to the external electron acceptor. Some aspects of this mechanism are still under debate. For instance, a revised mechanism has been recently suggested where CO₂ is inserted into a Ni(II)-hydride

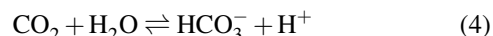
bond¹⁹. A second active site, a [Ni₂Fe₄S₄] cluster in the α subunit (the A cluster), catalyses the incorporation of the CO in a methyl group to give acetyl-CoA.



The ACS (α) and CODH (β) subunits of the bifunctional enzyme are associated in a dimer of dimers (α₂β₂). The C and A clusters are 70 Å apart from one another and a 138 Å long cavity runs along the entire length of the enzyme, connecting all A clusters and C clusters, from the sites where CO is produced to the sites where it is consumed.

2.3 Carbonic anhydrase II (CA II)

This enzyme is a small protein (29 kDa) which catalyses CO₂ hydration and HCO₃⁻ dehydration:^{20,21}



It is involved in many biological processes, such as maintaining the correct acidity of blood in mammals. It is also important in photosynthesis since the substrate of RubisCO, the enzyme involved in the first major step of carbon fixation, is CO₂ and not its hydrated forms. The active site of CA II is a Zn²⁺ centre coordinated by three His nitrogen and one water molecule (fig. 2D).

3 Methods

3.1 A general introduction to computational methods: calculations of structures (geometry, distances) and spectroscopic properties

Two strategies can be followed for the definition of QM models of metalloproteins. In the cluster approach, only the active site and some neighbouring atoms are taken into account, and the rest of the protein environment is only implicitly modelled. In the QM/MM approach, the active site is described using quantum chemistry, whereas all other atoms of the protein are modelled using a molecular mechanics formalism. Both approaches have advantages and disadvantages, which have been extensively discussed in recent reviews^{22–26}. The cluster approach is generally well suited for modelling metalloenzymes, since the chemical steps of the catalytic mechanism usually involve only the metal ions and nearby residues^{27–30}. However, the selection of the atoms included in the model is often far from trivial. In addition, the modelling of the peripheral atoms (i. e. those at the boundary of the QM model) can be problematic.

374 When a cluster model is used, the presence of the protein
375 matrix that surrounds the active site is generally modelled by
376 soaking the QM portion in a continuum dielectric. This is
377 particularly important for metal-containing active sites, which
378 often are not electrically neutral. In fact, an unbalanced charge
379 distribution in the active site can result in unrealistic electron
380 transfers within the model cluster. As a continuum dielec-
381 tric, several solvation models like the conductor-like screening
382 model (COSMO)^{31–34} and the polarizable continuum model
383 (PCM) have been developed.^{35–40}

384 When the architecture and stereoelectronic features of the
385 protein matrix are expected to affect the structural properties
386 of the active site, as well as the regiochemistry of substrates
387 or inhibitors binding, modelling the protein environment in
388 an explicit manner can be very important. The development
389 of QM/MM models, which has allowed the investigation of
390 whole proteins, was pioneered by Warshel and Levitt.⁴¹ These
391 methods have become increasingly popular in the last twenty
392 years.

393 The structures of organic molecules calculated with DFT,
394 which is the only affordable level of theory when dealing with
395 large systems, can be very reliable, with errors on bond dis-
396 tances and angles that are generally lower than 2 pm and a few
397 degrees. Regarding coordination compounds, strong metal
398 ligand bonds (such as those involving CO and CN⁻ ligands)
399 are generally predicted with excellent accuracy, whereas the
400 prediction of weaker metal-ligand bonds can be more prob-
401 lematic. Very weak interactions like hydrogen bonds can also
402 be challenging.

403 DFT calculations have been useful also for the elucidation
404 of structural properties of proteins. The so-called quantum re-
405 finement approach is a crystallographic refinement procedure
406 in which a molecular mechanics force field, which is gener-
407 ally used to supplement the X-ray diffraction data, is replaced
408 with more accurate DFT calculations⁴²; it has been used to
409 clarify the chemical structure of cofactors or the protonation
410 state of aminoacids. As an example, the nature of the dithio-
411 late ligand in the active site of [FeFe]-hydrogenases (fig. 2B)
412 was initially controversial, since it was suggested that it may
413 contain C, N, or O as the bridgehead atom. To shed light on
414 this issue, Ryde and collaborators⁴³ carried out quantum re-
415 finement calculations taking into account different models of
416 the dithiolate ligand, finding that structures with a N bridge-
417 head atom provide the best fit to the raw crystallographic data,
418 in agreement with previous proposals^{44–46}. These results were
419 confirmed recently when it became possible to change the na-
420 ture of the bridging dithiolate ligand¹⁶: the enzyme is active
421 only if the bridging ligand bears a nitrogen atom.

422 It is also important to keep in mind that metalloproteins of-
423 ten contain metal ions with unpaired electrons, which must be
424 described using spin polarized methods, where electrons with
425 different spin are treated with a different potential. In addi-

426 tion, in some enzymes, such as those containing [4Fe4S] clus-
427 ters, the metal atoms can interact, generating antiferromag-
428 netic coupling between electrons localized on different atoms.
429 Spin-coupled systems are intrinsically difficult to describe us-
430 ing DFT because their ground state wavefunctions generally
431 correspond to linear combinations of multiple determinants.
432 However, approximate methods have been shown to produce
433 reliable results: in the broken symmetry (BS) approach de-
434 veloped by Noodleman and coworkers^{47,48} the opposite spins
435 are localized to give a mono-determinant representation of the
436 spin exchange interactions within the molecule.

437 The prediction of vibrational frequencies, and consequently
438 of IR spectra, is closely related to the accuracy in the calcula-
439 tion of equilibrium geometries. In general, harmonic frequen-
440 cies computed using DFT, when scaled using *ad hoc* empirical
441 correction factors, agree very well with experimental data and
442 can allow to distinguish among different plausible chemical
443 structures that might correspond to the species under investi-
444 gation. As an example, the combination of data obtained from
445 infrared (IR) spectroscopy with the corresponding computed
446 spectra has been one of the most effective approaches used to
447 characterize hydrogenases. In fact, the peculiar presence of
448 CO and CN⁻ ligands in the active site of these enzymes has
449 allowed to monitor the shifts of their vibrational modes and to
450 correlate them with the molecular structure of different redox
451 and protonation states of the enzyme^{49–51}.

452 The calculation of other spectroscopic properties, such as
453 UV-Vis, CD and EPR, is more challenging and high-level *ab*
454 *initio* methods, such as CCSD(T) and CASSCF, are often re-
455 quired to obtain reliable results. However, as these meth-
456 ods are computationally very expensive, theoretical chemists
457 make extensive use of DFT to compute spectroscopic proper-
458 ties of bioinorganic systems^{24,52,53} and the performance and
459 reliability of this method has recently been discussed⁵⁴. In
460 general, computed spectroscopic properties obtained using
461 DFT are not always accurate, and sometimes even qualitative
462 results can be incorrect. For this reason, DFT derived prop-
463 erties must be carefully checked and tuned using experimen-
464 tal data as reference. DFT calculations of Mössbauer isomer
465 shifts for the ⁵⁷Fe nucleus have generally produced encourag-
466 ing results⁵⁵. In contrast, the computation of EPR parameters
467 is more problematic. Indeed, *g*-shift values are often under-
468 estimated when using standard functionals, and some metal
469 ions, such as Cu(II), can be particularly challenging. The ac-
470 curate prediction of hyperfine coupling constants can also be
471 difficult, with results that can be strongly dependent on the na-
472 ture and oxidation state of the metal ion under investigation.
473 Nevertheless, DFT calculations of *g* values and hyperfine cou-
474 pling constants have often well complemented data obtained
475 from EPR spectroscopy, as documented by their role in the
476 characterization of structural features of paramagnetic [NiFe]-
477 hydrogenase forms¹².

478 Since only electronic ground states can be rigorously com-
 479 puted using DFT calculations, the investigation of excited
 480 states and their properties can be carried out only indirectly. In
 481 this context, DFT has benefited from the development of time-
 482 dependent linear response theory within the *ab initio* methods.
 483 Time-dependent density functional theory (TDDFT) is now
 484 routinely applied to compute the electronic spectra of bioinor-
 485 ganic systems, even though the quality of the results is very
 486 dependent on the molecular system under investigation and
 487 on the choice of the exchange-correlation functional. Multi-
 488 configurational approaches, such as CASPT2 and MRCI, can
 489 give more accurate results, but these methods are still compu-
 490 tationally very expensive.

491 3.2 Calculating and measuring thermodynamic param- 492 eters.

493 3.2.1 Energy and free energy profiles (intermediates and 494 Michaelis complexes)

495 QM calculations can give quantitative information about the
 496 thermodynamics and the kinetics of a reaction pathway,
 497 through the computational characterization of the structure of
 498 reactants, products, intermediate species and the correspond-
 499 ing transition states, as well as their energy differences. While
 500 the computation of the structures of reactants, intermediate
 501 species and products is relatively straightforward, because
 502 they correspond to energy minima on the potential energy sur-
 503 face, the computation of transition states (TSs) in a reaction
 504 pathway (i.e. saddle points on the potential energy surface)
 505 requires deep chemical intuition, because they cannot be de-
 506 duced unambiguously just from the specification of reactants
 507 and products⁵².

508 Standard reaction energies of organic molecules, such as
 509 additions and substitutions, when computed with DFT meth-
 510 ods, are generally within 2–3 kcal/mol of the corresponding
 511 experimental values. The level of accuracy slightly decreases
 512 when considering bioinorganic systems containing transition
 513 metals, but the trade-off between accuracy and computational
 514 costs remains extremely good, allowing to cautiously discuss
 515 and compare computed reaction energies. As an example, an
 516 average accuracy of about ± 5 kcal/mol can be expected in the
 517 computation of metal-ligand dissociation energies⁵². How-
 518 ever, it is important to remark that an error of 1.4 kcal/mol in
 519 binding energies corresponds to an order of magnitude differ-
 520 ence in K_d at room temperature; the same problem arises in
 521 attempts to deduce rates from activation energies. Also due to
 522 the approximations necessarily introduced to model large bio-
 523 logical molecules, the discrimination among alternative reac-
 524 tion pathways only on the basis of energy differences between
 525 intermediates and transition states can be problematic. In fact,
 526 for some difficult cases, such as Cu_2O_2 or Fe(IV)-oxo contain-
 527 ing systems, even a qualitative analysis might lead to wrong

conclusions²⁴. In addition, to describe the energy profile of
 a reaction, standard free energy differences (ΔG^0) should be
 computed, whereas QM calculations provide directly only the
 electronic energy differences (ΔE^0). The comparison of ΔE^0
 values is sufficient to discriminate among different reaction
 pathways when the energy corrections that should be com-
 puted and added to ΔE^0 to obtain the corresponding ΔG^0 val-
 ues can be assumed to be similar for the different reaction
 pathways under investigation. Experimental observables are
 free energies, but their computation is often affected by large
 errors. First, computed energies should be corrected with
 the vibrational zero-point energy (ZPE) contribution, which is
 crucial if the aim is to compute deprotonation energies⁵⁶ or to
 evaluate proton-transfer energies and barriers, proton tunnel-
 ing, and kinetic isotope effects.^{57,58} Second, entropic contri-
 butions should be taken into account, and calculated from the
 roto-translation partition function of the system, at a given T
 and P . However, only approximated partition functions can be
 computed for molecules containing a large number of atoms.
 Of course, entropic corrections are crucial for the description
 of associative and/or dissociative elementary reaction steps;
 their values are in the range of +10 kcal/mol for an associative
 reaction step, when considering standard state concentrations.

Regarding experiments, among the various quantities
 which are related to free energy variations, only associa-
 tion/dissociation constants and reduction potentials can be
 easily measured (if we exclude equilibrium constants between
 substrate and product and reaction energies, which give no in-
 formation about the catalyst). This is described hereafter.

527 3.2.2 Experimental dissociation constants

528 Many experimental methods make it possible to measure ei-
 529 ther equilibrium dissociation constants between enzyme and
 530 ligands (hence free energies of binding) or apparent dissocia-
 531 tion constants for the reaction



533 The main issues in interpreting these results are that not all
 534 parameters in units of concentration are true dissociation con-
 535 stants (related to a free energy of binding), and that the differ-
 536 ent parts of the system that contribute to the apparent affinity
 of the enzyme for a ligand are difficult to resolve.

537 If one is interested in the catalytic transformation of a sub-
 538 strate S into a product P, the change in steady state turnover
 539 rate against substrate concentration can often be understood
 540 from a very simple scheme:



An experimental parameter that is easily measured is the Michaelis constant, K_m , defined from the change in turnover frequency (ν) against substrate concentration:

$$\nu = \frac{\nu_{\max}}{1 + K_m/[S]} \quad (7a)$$

$$K_m = \frac{k_{\text{cat}} + k_{\text{out}}}{k_{\text{in}}} \quad (7b)$$

The Michaelis constant is greater than the true dissociation constant $K_d = k_{\text{out}}/k_{\text{in}}$ unless the transformation of the enzyme-substrate complex is slow compared to substrate release⁵⁹ and $K_m = K_d$.

True dissociation constants are more easily obtained from inhibition experiments. If the inhibition by a certain ligand is *reversible*, then the turnover rate reaches a non-zero, steady-state value in the presence of substrate and inhibitor, and the inhibitor binding constant is deduced by looking at how the steady-state turnover rate ν changes with inhibitor concentration [I]:

$$\nu = \frac{\nu([I] = 0)}{1 + [I]/K_i^{\text{app}}} \quad (8)$$

The apparent dissociation constants K_i^{app} can also be deduced from the ratio of experimentally determined binding/dissociation rate constants. It may depend on substrate concentration. For example, if the substrate and the inhibitor compete for binding to the same active site,⁶⁰ then the apparent K_i measured by changing [I] at a constant [S] is

$$K_i^{\text{app}} = \frac{K_i}{1 + [S]/K_m} \quad (9)$$

If the inhibitor reversibly binds to form a dead-end complex, as occurs with CO binding to hydrogenase for example, then inhibitor binding is at equilibrium in the steady-state⁵⁹, and the measured K_i is a true thermodynamic parameter. H_2 inhibits proton reduction in both [NiFe]- and [FeFe]-hydrogenases (the former more strongly than the latter). However, the enzyme- H_2 complex is not a dead-end (it is a catalytic intermediate of H_2 evolution) and therefore the inhibition constant is not a true dissociation constant; it is actually greater than K_d (ref. 61).

If the inhibitor binds *irreversibly* on the experimental time scale, then inhibition is complete (provided the concentration of inhibitor is greater than the concentration of enzyme) and the rate of inhibition can be measured,⁹ but the rate constant of dissociation and the dissociation constant (K_d) cannot.

3.2.3 Reduction potentials

Reduction potentials are very important properties of redox cofactors, because according to Marcus theory, they are one

of the three parameters that determine the kinetics of electron transfer (ET) between distant centers. The other two are the reorganisation energy, which is difficult to measure (it is deduced from the dependence of the rate of ET on either ΔG or T , all things being equal), and the intercenter coupling, which cannot be independently measured. Note however that when both redox centers are paramagnetic, the intercenter coupling is related to the magnitude of their exchange interaction, which can be deduced from the simulation of the EPR spectrum⁶². The reduction potential of an active site is also one of the parameters (but by no means the only parameter) that determines the “catalytic bias”, that is whether the enzyme is a better catalysts of the reaction in the oxidative or reductive direction^{5,63}.

Reduction potentials can be determined in experiments termed redox titrations, where the system is poised under equilibrium conditions, stepwise reduced or oxidized; the “solution” potential is measured using a platinum electrode and the redox state is monitored using a spectroscopic technique. This is conceptually very simple if the system has a single redox center. If the protein or enzyme houses several redox centers that interact (meaning that the reduction potential of one center is affected by the redox state of the nearby centers), it is important to distinguish between microscopic reduction potentials (that can only be measured if the centers have distinct spectral properties) and macroscopic potentials (that are measured if the centers are indistinguishable in a particular experiment)^{1,64}.

Depending on the spectroscopic method used to monitor the redox state of the sample and the spectral properties of the redox cofactors, a large amount of biological material may be required to carry out a complete redox titration. The implementation of the measurement is often tricky. (1) A cocktail of redox mediators has to be present in solution to increase the rate at which the equilibrium is reached; its composition and concentration must be chosen carefully. (2) An artifact may arise from the fact that the redox equilibrium may unexpectedly shift when the sample is frozen to be examined by e.g. EPR (for an effect of temperature on the thermodynamics of intramolecular ET, see e.g. ref 65). Changes in apparent pH can also occur on freezing aqueous buffer solutions⁶⁶. (3) Enzymes like hydrogenases cannot be equilibrated at low potential because they turnover protons, which cannot be removed from the solution. (4) Last, and maybe most importantly, it is rarely checked that the redox process is fully reversible (for an example where it is unexpectedly irreversible, see ref. 67). Overall, the error on E^0 is most often larger than ± 10 mV, and there are many sources of artifacts that can result in the value being uncertain.

Dynamic electrochemical methods, where the system is not at equilibrium, can also be used to measure reduction potentials.⁶⁸ The information can sometimes be simply obtained

661 from the result of a voltammetric experiment, where the elec- 711
 662 trode potential is repeatedly swept up and down to trigger the 712
 663 oxidation and reduction of the center, which is detected as a 713
 664 oxidation or reduction current. If the system has several redox 714
 665 centers, voltammetry measures macroscopic reduction poten- 715
 666 tials. If the redox reaction is a pure electron transfer or if it is 716
 667 coupled to fast reversible reactions (such as (de)protonation or 717
 668 ligand binding and release), then the thermodynamic informa- 718
 669 tion is easily obtained from experiments carried out in the low 719
 670 scan rate limit, where the system remains close to equilibrium. 720
 671 The rate of interfacial electron transfer and/or the rates of the 721
 672 coupled reactions can be deduced from experiments carried 722
 673 out at fast scan rates⁶⁹. If the coupled reaction is irreversible, 723
 674 then the reduction potential can only be measured if the elec- 724
 675 trode potential is swept so quickly as to outrun the coupled 725
 676 reaction⁷⁰, but there is no guarantee that this regime can be 726
 677 reached in experiments. 727

678 If the coupled reaction is the reversible or irreversible cat- 728
 679 alytic transformation of a molecule in solution, then the elec- 729
 680 trochemical response we are considering is a catalytic current, 730
 681 which is proportional to turnover frequency. If we consider the 731
 682 situation where electron transfer between the electrode and the 732
 683 enzyme is direct, the mid-point potential of the catalytic wave 733
 684 is somehow related to the reduction potential of the enzyme's 734
 685 active site, but it is *equal* to the reduction potential of the ac- 735
 686 tive site only in very rare situations. In most cases, the wave 736
 687 potential (the "catalytic potential") is a global parameter that is 737
 688 affected by the thermodynamics⁷¹ and kinetics⁷² of substrate 738
 689 binding, the kinetics and thermodynamics of intramolecular 739
 690 electron transfer along the redox chain that wires the active 740
 691 site to the electrode^{4,5}, the kinetics of electrode/enzyme elec- 741
 692 tron transfer⁷³ etc. It is now clear that catalytic potentials are 742
 693 parameters that may strongly depart from the reduction po- 743
 694 tential of the active site. An analogy in this respect is the 744
 695 Michaelis constant, which has the unit of a dissociation con-
 696 stant, but is not a thermodynamic parameter (cf eq. 7b)⁵⁹.

697 The comparison of experimental and calculated reduction 745
 698 potentials may help understand how the environment tunes the 746
 699 redox properties of a metal center. Calculating potentials may 747
 700 also discriminate between several plausible mechanisms. The 748
 701 reduction potential is directly proportional to the free energy 749
 702 change associated to the redox process: 750

$$\Delta G = \Delta E_{\text{el}} + \Delta G_{\text{solv}} + E_{\text{zpe}} - RT \ln(q) \quad (10)$$

703 where ΔE_{el} is the adiabatic electron affinity of the system at 751
 704 the potential energy minimum of the oxidized state, ΔG_{solv} is 752
 705 the difference in solvation free energies of the oxidized and 753
 706 reduced forms, and E_{zpe} and $RT \ln(q)$ are the enthalpic and 754
 707 entropic contributions for the optimized structure, calculated 755
 708 within the harmonic oscillator/rigid rotor approximation. Due 756
 709 to the difference in charge between reactants and products, re-
 710 duction potentials are generally strongly affected by the envi-

711 ronment. Regarding coordination compounds, the differences 712
 713 in the solvation free energies of the reduced and oxidized 714
 715 species are usually computed using implicit solvation models, 716
 717 such as PCM, COSMO and COSMO-RS^{24,74}, and their reduc- 718
 719 tion potentials can often be accurately computed using DFT 719
 720 methods (although complications arises in some class of com- 720
 721 pounds, see as an example some Cu complexes). Such calcu- 721
 722 lations are more problematic in the case of metalloenzymes, 722
 723 because the environment of the redox centre cannot be satis- 723
 724 factorily described using an implicit solvation model. There- 724
 725 fore, the intermolecular interactions between the active site 725
 726 and the environment must be described with QM/MM meth- 726
 727 ods where the effect of the inhomogenous dielectric environ- 727
 728 ment is treated at an atomistic level. In addition, an adequate 728
 729 sampling of the configurations associated with the environ- 729
 730 mental degrees of freedom can be crucial, in particular when 730
 731 the active site is flexible or the surrounding residues adopt dif- 731
 732 ferent conformations. In such case the harmonic approxima- 732
 733 tion, which is usually assumed for calculation of vibrational 733
 734 entropy, is no longer justified. Adequate sampling can be 734
 735 achieved, for instance, with QM- and QM/MM-based molec- 735
 736 ular dynamics simulations by sampling the vertical electron 736
 737 affinity ΔE_{el}^v ⁷⁵⁻⁷⁹, 737

$$\Delta G = -kT \ln \langle \exp(\Delta E_{\text{el}}^v/kT) \rangle_{\text{O}} \quad (11)$$

738 where $\langle \rangle_{\text{O}}$ denotes the thermal average for the potential en- 734
 739 ergy surface of the oxidized state. Note that the expression 735
 740 above is a rigorous result of classical statistical mechanics and 736
 741 does include all enthalpic and entropic effects (corrections for 737
 742 nuclear quantum effects can be added). The thermal aver- 738
 743 age needs to be computed using enhanced sampling schemes 739
 744 such as free energy perturbation or thermodynamic integra- 740
 745 tion, which are computationally expensive. However, when 741
 746 the fluctuations of the ΔE_{el}^v are gaussian,^{78,80} it is sufficient 742
 747 to carry out two MD simulations (one in the reduced state and 743
 748 one in the oxidized state) and take the average of the two⁷⁷: 744

$$\Delta G = (\langle \Delta E_{\text{el}}^v \rangle_{\text{O}} + \langle \Delta E_{\text{el}}^v \rangle_{\text{R}}) / 2 \quad (12)$$

749 Even when QM- and QM/MM-based molecular dynamics 745
 750 approaches are used, the results are often affected by large er- 746
 751 rors. An error of 100 mV may not be acceptable considering 747
 752 that the biological redox scale is very narrow (most relevant 748
 753 reduction potentials range from -400 mV to +500 mV), and 749
 754 yet error of 100 mV corresponds to about 2.3 kcal/mol, which 750
 755 is well within the present accuracy of DFT methods. There- 751
 756 fore, results obtained from computing electron affinities, ion- 752
 757 ization energies and reduction potentials are often more use- 753
 758 ful in a relative or qualitative manner, to distinguish among 754
 759 different species or reaction paths, than for the prediction of 755
 760 absolute values. In other words, such calculations are most 756
 761 useful if one aims at understanding *changes* in the reduction 757

758 potential of a cofactor in response to point mutations or other
 759 modifications of the environment, or differences in the reduc-
 760 tion potential of the same cofactor in different proteins^{81,82}.
 761 In these cases, since the QM system containing the redox ac-
 762 tive co-factor is the same and changes in reduction potential
 763 are due to different interactions with the environment only,
 764 the DFT errors are expected to cancel. Indeed, one can as-
 765 sume that the reduction potential differences are mostly due
 766 to the protein so that a QM calculation is no longer neces-
 767 sary and the reduction potential can, to first approximation,
 768 be calculated entirely with classical force fields^{81,82} or contin-
 769 uum electrostatics methods⁸³. A recent example is the calcu-
 770 lation of the relative reduction potentials of ten identical *c*-type
 771 heme cofactors bound to the deca-heme protein MtrF⁸², as re-
 772 viewed in another article of this issue⁸⁴. In this study classical
 773 MD simulation was employed to compute the reduction poten-
 774 tial using thermodynamic integration. The range of potentials
 775 computed was in relatively good agreement with experiment,
 776 even though the computed potentials were microscopic reduc-
 777 tion potentials (all other hemes remaining oxidized), whereas
 778 in experiments (protein film voltammetry) macroscopic reduc-
 779 tion potentials are measured (the system goes from being fully
 780 oxidized to fully reduced as the electrode potential is swept
 781 down). The effect of the oxidation state of a neighbouring co-
 782 factor on the reduction potential can be significant, in the order
 783 of 10 to 95 meV^{85–87}, but it remains typically below the statis-
 784 tical error caused by the finite length of the MD trajectories.

785 3.2.4 Acidity constants

786 Protein folding and stability, as well as many biological pro-
 787 tein functions such as proton and electron transfer processes,
 788 ligand binding, and protein-protein association, are controlled
 789 by the ionization state of protein side chains. The pK_a s of
 790 such acidic or basic side chain (Asp, Glu, Lys, Arg, His) are
 791 strongly affected by the protein environment, so that they can
 792 be significantly different in the protein with respect to the
 793 value of the amino acid in solution.⁸⁸ This is particularly true
 794 for ionisable groups buried in a hydrophobic pocket. An ex-
 795 ample is given by the pK_a value measured for a Lys residue in-
 796 serted in the hydrophobic core of staphylococcal nuclease by
 797 site-directed mutagenesis,^{89–91} which is 4.3 units lower than
 798 the pK_a of Lys in water: this residue is deprotonated in the
 799 protein.⁹²

800 Several experimental methods, such as equilibrium denatu-
 801 ration measurements at different pH and potentiometric titra-
 802 tions have been applied to evaluate pK_a s of ionisable residues
 803 in proteins. Accurate values of pK_a s can be measured us-
 804 ing multidimensional and multinuclear NMR spectroscopy, by
 805 monitoring the pH dependence of ¹³C, ¹H and ¹⁵N chemical
 806 shifts and corresponding coupling constants of relevant atoms
 807 (C γ for Asp; C δ for Glu; C δ , C δ 2, N ϵ 2 and N δ for His, etc.)

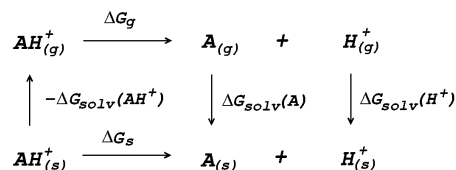


Fig. 3 Thermodynamic cycle for the calculation of deprotonation Gibbs free energy in solution (ΔG_s).

previously assigned to specific residues.^{92–95}

Theoretical predictions of pK_a s are very useful even when experimental values are available, since they can provide a better understanding of the molecular determinants of ionization. Many different methods and levels of theory have been proposed for the calculations of pK_a s.⁹⁶ However, in spite of the significant progress since the first work of Tanford and Kirkwood based on the Poisson-Boltzmann equation⁹⁷, calculation of pK_a s remains challenging because of the difficulties in capturing quantitatively the effects of the strong and position dependent short-range electrostatic interactions, and the nonspecific long range interactions between charged sites and with the solvent.^{98–100}

The heterogeneous response of the protein to a change in charge, which depends on the dielectric environment and the local flexibility, is another difficult issue^{101–103}. As recently reviewed, among the various methods proposed for pK_a calculations, none performs significantly better than others.⁹⁶

The most fundamental approach for describing electrostatics, as well as all other physical interactions, are quantum mechanical (QM) methods which solve the Schrödinger equation at some level of approximation. This approach can be successfully applied to small molecular systems such as single amino acids or small peptides.^{104–108} In this case full QM geometry optimizations and vibrational frequencies calculations are carried out for the species included in a thermodynamic cycle such as that in fig. 3.

The Gibbs free energy of reaction in solution (ΔG_s) is obtained as the sum of the Gibbs free energy of reaction in vacuum (ΔG_g) and the difference in solvation free energies ($\Delta\Delta G_{\text{solv}}$)

$$\Delta G_s = \Delta G_g + \Delta\Delta G_{\text{solv}} \quad (13)$$

where $\Delta G_g + \Delta\Delta G_{\text{solv}}$ are calculated as:

$$\Delta\Delta G_{\text{solv}} = \Delta G_{\text{solv}}(\text{A}) + \Delta G_{\text{solv}}(\text{H}^+) - \Delta G_{\text{solv}}(\text{AH}^+) \quad (14)$$

$$\Delta G_g = G_g(\text{A}) + G_g(\text{H}^+) - G_g(\text{AH}^+) \quad (15)$$

pK_a values can then be calculated from ΔG_s using the equation:

$$K_a = \exp \frac{-\Delta G_s}{RT} \quad (16)$$

The main source of errors in this approach seems to arise from modelling solvation. In particular, widely used dielectric continuum models (DCM) are frequently the worse approximation for systems where short range solute-solvent interactions are important. The explicit inclusion of a few solvent molecules in close proximity to the solute in addition of using a DCM can be a way to overcome this issue, without making the calculations computationally too expensive.¹⁰⁹ In this respect we note that more elaborate DFT based molecular dynamics schemes have been developed for calculations of pK_a values, where both the solute and a large number of solvent molecules are treated at the DFT level.¹⁰⁸ In addition, the accuracy of the calculated pK_a s is also significantly improved by using thermodynamic cycles that maximize systematic error cancellations.¹¹⁰ The QM level of theory used in the pK_a calculations is also important, as it should be feasible at reasonable computational costs for relatively large-sized systems.

For macromolecular systems like proteins, using a QM method for the entire system is clearly prohibitive due to the computational cost. Most importantly, the use of QM methods is undesirable since electrostatic interactions dominate at large distances, and must be included in the calculation. An approach to overcome these issues is the QM/MM method introduced in section 3. In this context, *ad hoc* computational methods for the calculation of pK_a s have been recently proposed by Li and Jensen and coworkers:^{111,112} one method is based on a QM representation of the ionisable residues and their immediate environment combined with a continuum description of bulk solvation with the linear Poisson-Boltzmann equation; alternatively, the QM region is surrounded by fragments described by static potentials predetermined using *ab initio* QM.

Several methods utilizing Molecular Dynamics (MD) and Monte Carlo (MC) simulations have recently been proposed at various levels of approximation. We recall that MD simulations are used to sample all possible conformations of a protein by calculating a long trajectory based on deterministic rules (Newton mechanics) whereas MC simulations consist in randomly generating a large number of conformations, which are accepted or rejected according to their Boltzmann probability. Recent promising models combine (i) atomistic simulations of the protein, performed using MC or MD with a fixed or flexible protein backbone, (ii) an implicit description of the solvent using a Poisson-Boltzmann model (PB), and (iii) a MC sampling of conformations and ionization states of the protein. In these PB based approaches, the protein is defined as a region with a low dielectric constant embedded in a solvent with a high dielectric constant. The value of the dielectric constant of the protein is crucial for the correct prediction of pK_a s. In this respect, different values have been used, from 4 to 80,^{113–116} as the appropriate value depends on the distribution of polar and charged residues within the protein and on

local protein flexibility.^{117–119}

One of the most commonly used methods for incorporating conformational flexibility into pK_a calculations is the so-called Multi-Conformation Continuum Electrostatics (MCCE) method developed by Alexov and Gunner.^{114,119} In the MCCE the protein side chain flexibility is considered by generating several conformations for each residues which are relaxed using a force field with Lennard-Jones and torsion energies. The resulting conformers, which represent all degrees of freedom including appropriate acid/base ionization states and side chain positions, are then subjected to Monte Carlo sampling to generate the Boltzmann distribution of conformers. A state featuring one conformer for each residue is a microstate. The energy expression to determine the acceptance for a microstate x (ΔG^x) is given by:

$$\Delta G^x = \sum_i^M \delta_{x,i} \left[2.3 m_i k_b T (pH - pK_{sol,i}) + \Delta G_p + \sum_{j=i+1}^M \delta_{x,j} (\Delta G_{ij}^{CE} + \Delta G_{ij}^{LJ}) \right] \quad (17)$$

where M is the total number of conformers, $\delta_{x,i}$ is 1 if conformer i is present in the microstate and 0 otherwise, m_i is 1 for bases, -1 for acids and 0 for neutral conformers, $k_b T$ is 0.59 kcal/mol at 298 K, $pK_{sol,i}$ is the reference value of pK_a for the group involved in the ionization equilibrium, ΔG_p is a sum of pairwise terms independent from the other conformers of the microstate, and ΔG^{CE} and ΔG^{LJ} are pairwise electrostatic and Lennard-Jones energy terms which depend on the conformers selected in the microstate. Monte Carlo simulations are carried out for 15 different values of pH. The pK_a of each ionizable group is then calculated from the occupancy of the ionized form in the Boltzmann distribution using the Henderson Hesselbach equation:

$$\langle Occ_{ionized} \rangle = \frac{10^{-mn(pH-pK_a)}}{1 + 10^{-mn(pH-pK_a)}} \quad (18)$$

in which m is equal to -1 for an acid and 1 for a base and n is the Hill coefficient reflecting the degree of cooperativity between different sites.

Equilibrium ionization states in proteins have also been investigated by the protein dipole Langevin technique,^{103,120} and by MD based approaches using either constant-pH MD or free energy perturbation techniques.^{121–124}

3.3 Kinetic parameters

3.3.1 General comments

The ability of an enzyme to catalyze a certain reaction is most easily quantified by the Michaelis parameters, K_m and k_{cat} (or

v_{\max} , see eq. 7a), obtained by fitting the dependence of steady-state turnover rate on reactants concentration. The Michaelis parameters are “global” parameters, which depend on all steps in the mechanism and usually tell us very little about the mechanism and the rates of particular steps in the catalytic cycle (such as intramolecular electron or proton transfers) unless it is clearly established that one particular step fully limits turnover (about the concept of rate limiting step, i.e. the step which, if perturbed, causes the largest change in overall velocity, see the discussions of pitfalls in ref. 125,126). An example discussed in section 4 is carbonic anhydrase, where proton transfer is the rate limiting step in turnover, but there are also examples where intramolecular electron transfer (ET) is rate limiting⁶⁵. To specifically learn about individual steps, the experimental method consists in triggering the cycle and monitoring the evolution of the concentration of reaction intermediates by appropriate techniques, most often spectroscopic techniques. A kinetic model is then needed to deduce the rate constants.⁸⁷ Another general approach consists in examining how the steady-state kinetic parameters are altered when the substrate or the system is modified, for example by changing the concentrations, temperature, substrate/solvent deuteration, or using site-directed mutagenesis. In that sense, the amino-acid sequence can be considered as one of the experimental parameters which can be varied to see an effect on rates.¹²⁷

In contrast, regarding complex metalloenzymes, the *calculations* of rates necessarily focus on one particular step, not the entire cycle. Since reaction rates are macroscopic averages over a very large number of reactive events from the reactant basin to the product basin (and vice versa), following different trajectories, it is necessary to compute a large number of trajectories (dynamics approach) or to use statistical theories based on ensemble distributions. In particular, using MD, the reaction rates can be computed by averaging a statistically representative number of trajectories, obtained using different initial conditions, that take reactants to products. Many approaches exist to carry out such averaging procedure in practice at a reasonable computational cost: “umbrella sampling” is one such method, where the potential energy surface is biased to force the trajectories computed by molecular dynamics simulations to reach the transition state region. The most used statistical approach is grounded in the transition state theory (TST) of Eyring, according to which

$$k = \kappa \frac{k_B T}{h} \exp \frac{-\Delta G^{0\ddagger}}{RT} \quad (19)$$

where $\Delta G^{0\ddagger}$ is the standard free energy of activation, directly evaluated from the barrier height, i.e., from the energy difference existing between the transition state and the preceding intermediate. However, due to the present accuracy of theoretical methods and to the approximations used to compute free energies, the comparison between computed and exper-

imental reaction and activation energies is often only semi-quantitative. Equation 19 includes a prefactor, κ , that accounts for barrier recrossing, nuclear tunneling and dynamical effects¹²⁸.

In general, the enzyme kinetics is the result of a large number of elementary steps, most of them reversible, each occurring with a given rate constant. This includes not only the chemical reaction steps at the active site but also the transport processes of substrates/products. For instance, proton transfer from the solvent to buried active sites occurs via a chain of proton exchanges between water and/or protonatable amino acid residues (see section 3.3.2). Similarly, binding of small ligands to buried active sites can be described as a series of diffusive jumps between protein cavities connecting the solvent with the protein active site (see section 3.3.3). The time evolution of these kinetic chains can be obtained by solving master equations (a set of differential equations governing the time evolution of all possible states of the system) or by using kinetic Monte Carlo methods. The latter use as input the elementary rate constants obtained for each step, for instance, from TST.

3.3.2 Proton transfer (PT) rate constants

Direct information about the rate of a PT step in enzymes can be obtained when this step is rate limiting during turnover. This is expected when the catalytic constant k_{cat} is strongly modified either upon deuteration of the substrate or when the reaction is studied in D_2O (kinetic isotope effect, KIE). In this case, k_{cat} can be equated to the PT rate constant. In these circumstances, the activation free energy of the PT step can be deduced from the temperature dependence of k_{cat} . When the ΔpK_a of the proton transfer can be altered by modifying some ionisable groups or their environment, the variation of the PT rate constant as a function of ΔpK_a provides strong constraints for the interpretation of the PT mechanism (as exemplified with carbonic anhydrase, see section 4.4.3).

The rate of elementary proton transfer steps taking place in enzymes is generally calculated with the expression given by transition state theory (eq. 19).

To evaluate the activation free-energy $\Delta G^{0\ddagger}$, a suitable reaction coordinate is chosen so as to follow the reaction progress, like the difference between the donor-proton and acceptor-proton bond distances. Classical MD simulations with extensive umbrella sampling are then carried out to obtain the free-energy profile along the reaction coordinate (called PMF, potential of mean force). $\Delta G^{0\ddagger}$ can be obtained from the difference of the PMF at the maximum (transition state) and minimum (reactant state), see e.g. ref. 129 for details. The PMF also provides the standard free-energy change ΔG^0 , which is proportional to the ΔpK_a of the reaction. The parameters used in semiempirical methods must be determined through a care-

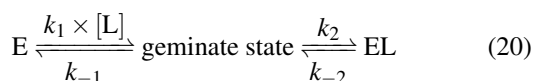
ful calibration based on a set of experimental data. Nuclear quantum mechanical effects due to tunnelling and zero-point energies may be significant in biological proton transfers. Various methods have been proposed to evaluate their contributions, especially in studies devoted to the interpretation of the KIE¹³⁰.

In enzymes, proton exchanges between the active site and the solvent take place through proton transfer chains made of protonatable groups, like water molecules and/or ionisable residues. The time evolution of these chains can be simulated by using various methods like the center of excess charge, the Langevin equation, or kinetic models leading to a master equation, as described in section 3.3.3.

3.3.3 Rates of ligand binding and release

Here we focus on methods for measuring and calculating the rates of binding of small ligands. In this context, the most intensively studied is CO diffusion in myoglobin, for which a wealth of experimental diffusion and binding rate constants are available for WT and mutant proteins¹³¹, but there has been considerable progress recently regarding intramolecular transport in hydrogenases and CO dehydrogenase.

In attempts to distinguish between the partition of the ligand between the solvent and the protein and the actual binding on the active site, it is useful to consider a two-step binding model, with the diffusion of the substrate towards a “geminate” (G) position near the active site (with a forward bimolecular constant k_1 and a first order rate of release k_{-1} , dissociation constant $K_1 = k_{-1}/k_1$) and the chemical binding/release on the active site (with first order rate constants k_2 and k_{-2} , equilibrium constant, $K_2 = k_{-2}/k_2$).¹⁰



The observed bimolecular rate of ligand binding and first order rate of ligand release are related to the four rate constants above by

$$k_{\text{in}} = \frac{k_1 k_2}{k_{-1} + k_2} \quad (21a)$$

$$k_{\text{out}} = \frac{k_{-1} k_{-2}}{k_{-1} + k_2} \quad (21b)$$

These equations are obtained by assuming (i) the steady state for G, $d[G]/dt = 0$ and (ii) that K_2 is small ($k_{-2} \ll k_2$).

In metalloenzymes that transform small molecules like CO, CO₂, and H₂, putative substrate tunnels are most easily identified as hydrophobic cavities in (static) X-ray structures. Xenon can be used as a probe in crystallographic studies, because it is supposed to prefer hydrophobic environments, like

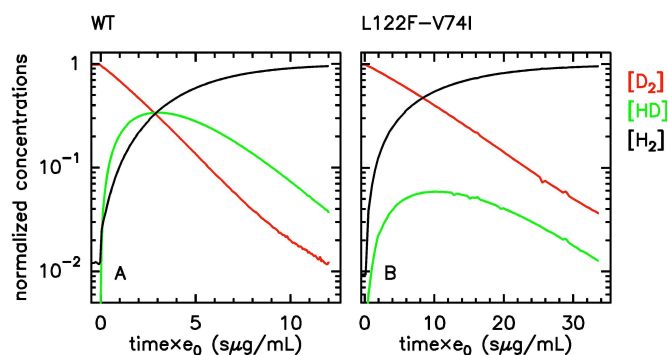


Fig. 4 Isotope-exchange assay (eq. 22) of the WT form (A) and L122F-V74I mutant (B) of *Desulfovibrio fructosovorans* [NiFe]-hydrogenase. The changes in concentrations are used to determine the rate of H₂ exit from the enzyme^{63,135}. e_0 is the concentration of enzyme. That the mutant produces less HD than the WT enzyme indicates that the mutation slows diffusion along the gas channel. Figure reproduced from ref. 63 (copyright 2012 American Chemical Society).

H₂ or O₂; it is of a similar size to O₂ but it is more electron-rich, thereby facilitating its detection with X-rays. We note that Xe-binding cavities may not reveal CO₂ diffusion paths because they may be too small to be used for CO₂ transport. Testing the diffusion pathways predicted from crystallographic studies usually consists in using site-directed mutagenesis to try to alter the main routes (most commonly, by increasing the bulk of the side chains that point in the channels) and examine the effect on the rates of ligand binding (see e.g. 132 for a review).

One method for probing the rate of intramolecular diffusion in enzymes may consist in measuring the rate of substrate or ligand binding in experiments where the enzyme-ligand complex has a clear UV-vis signature: the five-coordinate hemes of cytochrome *c* oxidase and myoglobin lend themselves to this sort of investigations.^{133,134}

Regarding hydrogenases, a particular method for looking at H₂ diffusion rates is based on analysing the progress of the isotope exchange reaction, whereby D₂ is irreversibly transformed into H₂ using protons from the solvent, in two steps that are catalyzed at the [NiFe] active site:



Both steps are irreversible, because the solvent H₂O provides a very large excess of H⁺ over D⁺. The reaction can be monitored by using mass spectrometry to follow the change in concentration of D₂, HD and H₂, see e.g. fig. 4. HD is an intermediate along the reaction pathway from D₂ to H₂, and because the egress of HD competes with its transformation into H₂, the

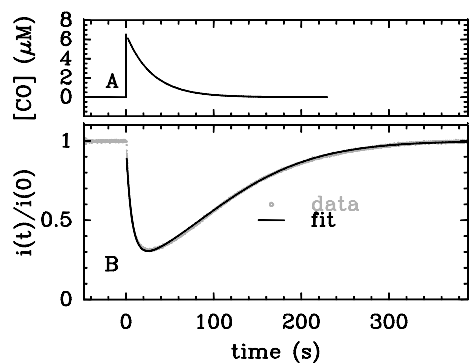


Fig. 5 Electrochemical monitoring of the inhibition by CO of H₂ oxidation by the L122M-V74M mutant of *D. fructosovorans* [NiFe]-hydrogenase where the double mutation slows diffusion along the gas channel. An aliquot of solution saturated with CO was injected at $t = 0$ and the change in current against time reveals CO binding and release. Panel A: CO concentration against time. Panel B: eq. 2 in ref. 60 is fit to the change in current against time (gray) to measure $k_{\text{in}}^{\text{CO, app}}$ and k_{out} . Figure reproduced from ref. 1 (copyright 2008 American Chemical Society)

1098 slower intramolecular transport, the less HD dissociates from
1099 the enzyme's active site and the less it can be detected in the
1100 solvent. Modelling the change in HD concentration against
1101 time returns the ratio of rate of HD dissociation over H⁺/D⁺
1102 exchange at the active site¹³⁵. Under certain conditions,⁶³ the
1103 data can also be used to directly measure the rate of dissociation,
1104 $k_{\text{out}}^{\text{H}_2}$.

1105 Alternatively, the information about the kinetics of ligand
1106 binding may be deduced from turnover-rate measurements: it
1107 is indeed possible to determine the rate of binding or release of
1108 a competitive inhibitor ("competitive" means that it targets the
1109 active site) by monitoring the change in turnover rate upon ex-
1110 posure to the inhibitor. The electrochemical measurement of
1111 the rate of binding and release of CO in hydrogenase is illus-
1112 trated in fig. 5: the H₂-oxidation activity is measured as a cur-
1113 rent, with the enzyme adsorbed onto an electrode immersed
1114 and rotated in a solution continuously flushed with H₂, and
1115 small aliquots of a solution saturated with CO are repeatedly
1116 injected in the cell.^{9,135} The concentration of CO instantly in-
1117 creases after each injection (the mixing time is about 0.1 s)
1118 and then decreases exponentially as CO is flushed away by
1119 the stream of H₂. The activity decreases after the addition of
1120 CO, and it is fully recovered as CO is flushed away by the
1121 stream of H₂.

1122 We derived in ref. 60 the analytical equation that can be
1123 used to fit the electrochemical data recorded after a single in-
1124 jection of CO to measure k_{out} and the apparent value of k_{in} .
1125 The value of $k_{\text{out}}^{\text{CO}}$ is independent of substrate concentration,
1126 but since H₂ competes with CO, the "true" value of k_{in} is ob-
1127 tained from its apparent value using:

$$k_{\text{in}}^{\text{CO}} = k_{\text{in, app}}^{\text{CO}} \left(1 + \frac{[\text{H}_2]}{K_m} \right) \quad (23)$$

1128 An alternative strategy for characterizing the kinetics of in-
1129 hibition by CO (or O₂) consists in fitting the exponential re-
1130 laxation of the catalytic current that follows a *step* in inhibitor
1131 concentration¹³⁶ (rather than a burst, as in fig. 5A). This can
1132 be achieved by injecting an aliquot of solution saturated with
1133 CO and simultaneously changing the composition of the gas
1134 phase above the cell solution. In that case however, it is im-
1135 portant to realize that the time constant τ of the relaxation is
1136 not $1/k_{\text{in, app}}^{\text{CO}}[\text{CO}]$, but it is:

$$\tau = 1 / \left(k_{\text{in, app}}^{\text{CO}} \times [\text{CO}] + k_{\text{out}}^{\text{CO}} \right) \quad (24)$$

1137 Unless the experiment consists in monitoring the spectro-
1138 scopic signature of the active site, the rates of diffusion in
1139 either direction (k_1^{CO} , k_{-1}^{CO}) and the rates of ligand binding
1140 and dissociation at the active site (k_2^{CO} , k_{-2}^{CO}) cannot be mea-
1141 sured independently, and the meaning of the binding/release
1142 rate constants must be discussed in relation to eq. 21.

1143 The rate of binding ($k_{\text{in}}^{\text{CO}}$) equates the rate of diffusion to-
1144 wards the active site only on condition that the binding at the
1145 active site is fast

$$k_{\text{in}}^{\text{CO}} = k_1^{\text{CO}} \quad \text{if} \quad k_2^{\text{CO}} \gg k_{-1}^{\text{CO}} \quad (25)$$

1146 In this case, the measured rate of ligand released (k_{out}) is the
1147 rate of diffusion out multiplied by the dissociation constant,

$$k_{\text{out}}^{\text{CO}} = k_{-1}^{\text{CO}} \times K_2^{\text{CO}} \quad (26)$$

1148 In other words, the dissociation from the active site acts as
1149 a pre-equilibrium for the release of the ligand, as discussed in
1150 SI of ref. 10.

1151 Atomistic simulations, in particular MD, have most often
1152 been used in this context independently of experimental in-
1153 vestigations. They can give important qualitative informa-
1154 tion on intramolecular transport, such as the most likely diffu-
1155 sion paths within the protein and the location of key residues
1156 that guide, block or gate ligand diffusion. The simulations
1157 that have been carried out were either based on long equilib-
1158 rium molecular dynamics¹³⁷⁻¹⁴⁰ or on the use of enhanced
1159 sampling methods¹⁴¹⁻¹⁴⁸. With computational capabilities
1160 steadily increasing in recent years, it has become possible to
1161 compute not only qualitative diffusion paths, but also energetic
1162 properties such as activation barriers^{146,147} and estimates of
1163 global free energy surfaces^{144,145,148}.

1164 Nevertheless, rate constants for the diffusion of gas
1165 molecules have only rarely been computed. Free energy sur-
1166 faces could in principle be used to obtain approximate diffu-
1167 sion rates using e.g. TST for each single transition. How-
1168 ever, as pointed out in ref. 131, there are two issues. First,

the transition of small ligands between protein cavities may be strongly affected by dynamical effects leading e.g. to frequent barrier recrossings. This effect is neglected in standard TST and calculation of respective correction factors for each transition would be cumbersome. Second, for the construction of free energy surfaces collective variables need to be chosen, typically the cartesian position of the gas molecule. While this is an intuitive and suitable choice for fast transitions, it may be a poor choice for slow transitions through narrow passages where gas diffusion is coupled to (“gated by”) side chain motions of amino acid residues. In this case the reaction coordinate for the diffusive transition is likely to be more complicated, involving in addition to the cartesian position of the gas molecule some suitable coordinates describing the motion of the side chain(s) in question.

Considering the above issues, it is preferable to compute diffusion rates directly without prior calculation of equilibrium free energy profiles. Indeed, for relatively small proteins like myoglobin, it has been possible to obtain estimates for diffusion rates by brute force MD simulations. In the work of ref. 138, a relatively large number of trajectories of length 90 ns were generated and the rate constants estimated by counting the number of successful transitions between solvent and active site. Similarly, in ref. 140, rates for CO migration between Xe-binding sites in myoglobin were estimated from equilibrium MD simulations. The results obtained for diffusion were combined with QM calculations for CO binding, to propose a detailed kinetic model that was in reasonable agreement with available experimental data.

Brute force MD simulations are sometimes insufficient to obtain a statistically significant number of successful transitions of gas molecules from the solvent to the enzyme active site. This can be the case for large gas-processing enzymes with active sites buried deep inside the protein, far away from the solvent. The large number of possible but unproductive pathways reduces the probability for successful entry in the active site. Other difficult cases are enzymes with very narrow passages for gas diffusion such as the [NiFe]-hydrogenase mutants studied in ref. 149. Some of us have recently developed a master equation approach with rate constants estimated from equilibrium and non-equilibrium MD simulation, that addresses the sampling problem in these systems^{150–153}. The method allows us to compute diffusion rates of small ligands, even when these are very slow. Most importantly, the approach yields phenomenological diffusion rate constants, that can be directly compared to experimental rate constants. In the following we describe this computational method in more detail.

In a first step, one runs one or several long equilibrium MD trajectory of the protein and the surrounding aqueous solution containing 10–100 gas molecules, in the following referred to as ligand (“L”). Small diatomic or triatomic molecules pen-

trate the protein typically on the pico- to nanosecond time scale and quickly explore the accessible cavities and tunnels inside the protein. In a second step, the equilibrium probability distribution of the gas molecules inside the protein is obtained by defining a grid and counting the number of times a molecule visits a given elementary volume. The probability distribution is then clustered (“coarse grained”) in a way such that the cluster positions coincide as closely as possible with the maxima of the probability distribution (see e.g. the spheres in fig. 7C). These clusters are then identified as coarse “states” in a kinetic model that describes ligand diffusion as a sequence of hops between these states with rate constants k_{ij} , where j is the initial state or cluster and i the final state. The surrounding solvent is considered as a single cluster with rate constants for transitions to protein clusters defined similarly. In a third step the transition rates k_{ij} are calculated simply by counting the number of transitions observed in the long equilibrium MD runs. For important transitions that are insufficiently sampled, enhanced sampling methods (such as e.g. non-equilibrium pulling) are used to obtain k_{ij} . In the fourth step the transition rates k_{ij} are inserted in a master equation, which is a set of coupled first order differential equations for the population of each cluster as a function of time, $p_i(t)$, with solution

$$p_i(t) = \sum_j (e^{t\mathbf{K}})_{ij} p_j(0) \quad (27)$$

where \mathbf{K} is the rate matrix with elements $[\mathbf{K}]_{ij} = k_{ij}$, $k_{jj} = -\sum_{i \neq j} k_{ij}$. The master equation 27 is solved for given initial conditions (e.g. by setting the gas population inside the protein to zero at time equal zero as is the case in experimental measurements) to obtain the time dependent population of the states as a function of time. For calculating the rate of diffusion to the active site, the quantity of interest is the ligand population in the geminate state, $p_G(t)$. In the fifth and last step $p_G(t)$ is fit to the phenomenological rate law for reversible diffusion of L to the enzyme active site



(first reaction step in eq. 20), which takes the form:

$$p_G(t) = \frac{k_1 [\text{L}]}{k_1 [\text{L}] + k_{-1}} [1 - \exp(-(k_1 [\text{L}] + k_{-1})t)] \quad (29)$$

Equation 29 relates the populations obtained with atomistic MD simulation techniques to the phenomenological rate constants for pure diffusion from the solvent to the active site and vice versa, k_1 and k_{-1} , respectively. Within the coarse master equation scheme described above it is straightforward to include the chemical binding step¹⁵³,



1262 For this, we define an additional “bound” state B, in which
 1263 the substrate is chemically attached to the enzyme (denoted as
 1264 EL in eq. 5 above) and the corresponding population p_B . The
 1265 rate constant for transition from state G to B, k_2 , and for the
 1266 reverse transition, k_{-2} , is estimated, for instance, using quan-
 1267 tum chemical methods as described above. The dimension of
 1268 the rate matrix in eq. 27 is then increased by one to include
 1269 the entries for k_2 and k_{-2} and eq. 27 is solved for p_B . A fit
 1270 of p_B to the phenomenological rate law for reversible ligand
 1271 attachment,



1272 takes the same form as eq. 29,

$$p_B(t) = \frac{k_{\text{in}}[L]}{k_{\text{in}}[L] + k_{\text{out}}} [1 - \exp(-(k_{\text{in}}[L] + k_{\text{out}})t)] \quad (32)$$

1273 and provides a route for calculating the phenomenological rate
 1274 constants for diffusion to the active site and chemical binding,
 1275 k_{in} and for chemical unbinding and diffusion out of the pro-
 1276 tein, k_{out} . Alternatively, the value of k_{in} can be calculated us-
 1277 ing the steady state formulae eq. 21 (note that in eq. 32, the
 1278 steady-state assumption for G is not made).

1279 In section 4 we will discuss applications of this method-
 1280 ology to substrate and inhibitor diffusion in hydrogenase and
 1281 ACS/CODH, and compare the rate constants computed this
 1282 way with experimental measurements.

1283 4 Case studies

1284 In this section we present selected examples taken from the
 1285 literature, to illustrate how the synergy between experimen-
 1286 tal kinetic studies and computational investigations can in-
 1287 form about the reactivity of complex metalloenzymes such as
 1288 [FeFe] and [NiFe]-hydrogenases, ACS/CODH and carbonic
 1289 anhydrase.

1290 4.1 [NiFe]-hydrogenase

1291 4.1.1 A peculiar [4Fe3S] cluster in O₂-tolerant [NiFe]- 1292 hydrogenases

1293 The interpretation of the X-ray diffraction data and spectro-
 1294 scopic signatures of metal cofactors in multicenter enzymes is
 1295 often nontrivial. In such cases the combination between exper-
 1296 imental and computational results can allow the characteriza-
 1297 tion of fine structural and electronic properties. An example is

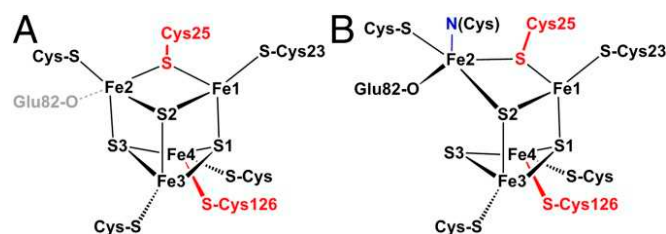


Fig. 6 Structure of the proximal [4Fe3S] cluster of the O₂ resistant [NiFe]-hydrogenase from *H. marinus*, in the reduced (3+) state (A) and in the superoxidized (5+) state (B). The two “supernumerary” cysteines, Cys25 and Cys126, are indicated in red, Glu82 in gray (A) or black (B). The cysteine closest to the [NiFe] site (Cys23), and the bond to the backbone nitrogen in the superoxidized state (blue), are also indicated. From ref. 156, copyright 2013 by National Academy of Sciences.

provided by recent studies carried out on O₂-tolerant [NiFe]-hydrogenases, which host an unusual proximal [4Fe3S] cluster (figure 6) and have attracted great attention due to the potential application of these enzymes in biotechnological energy-conversion processes^{154,155}.

To put the results below into context, it is important to remember that [NiFe]-hydrogenases are converted under oxidative (aerobic or anaerobic) conditions into a mixture of inactive states, two of which are referred to by the name or their EPR signatures: NiA and NiB¹⁵⁷. The enzymes recover H₂-oxidation activity upon reduction, NiB more quickly than NiA¹⁵⁸. According to X-ray investigations, an oxygenic ligand bridges the Ni and the Fe in the inactive states⁴⁵. The fact that the formation of NiA is favored when the enzyme is inactivated by O₂ under more oxidizing conditions (higher electrode potential, absence of H₂) has been taken as an indication that the oxygenic ligand in NiA is a peroxo produced upon incomplete reduction of the attacking O₂¹⁵⁹; however, this hypothesis was ruled out when control experiments showed that the amount of NiA is the same irrespective of whether the enzyme has been inactivated under aerobic or anaerobic conditions^{12,63}. Certain oxygen tolerant enzymes, which can oxidize H₂ in the presence of O₂, are inhibited by O₂ to form only a NiB state that is similar to that in O₂-sensitive hydrogenases except that it reactivates much more quickly^{160–162}. These enzymes house three high potential FeS clusters¹⁶³, including the very flexible, proximal [4Fe3S] cluster, which has been suggested to play a crucial role in the protection of the active site against oxidative inactivation. The [4Fe3S] cluster is linked to the protein by an unusual six-cysteine binding motif. Four of the six cysteine residues bind the cluster in the classical way, whereas one of the supernumerary cysteine residues replaces an inorganic sulfide in the cubane core, and the other is terminally coordinated to one of the Fe atoms. While classical [4Fe4S] clusters are involved in one-electron

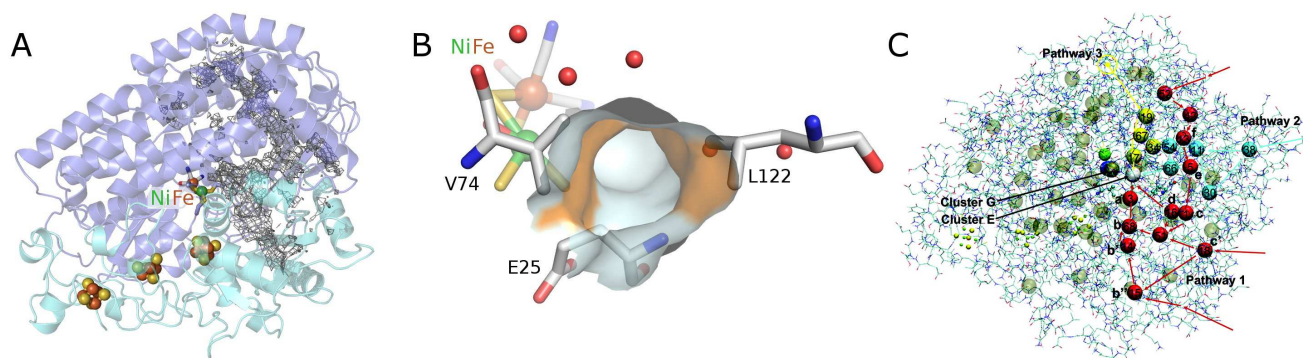


Fig. 7 Structure of *D. fructosovorans* [NiFe]-hydrogenase depicting the “dry” hydrophobic cavities. (A) The large and small subunits are shown as dark and light blue ribbons, respectively. Also shown are the active site, the chain of FeS clusters that wires the active site to the redox partners, and a grid delineating internal regions accessible to a probe of 1 Å radius. (B) Close up showing the access to the active site as the surface of the atoms that tile the end of the dry tunnel. Smaller, red spheres indicate the position of ordered water molecules in nearby “wet” cavities. Spheres in the background depict the Ni and Fe ions. Their ligands and residues Leu122, Val74 and Glu25 are shown as sticks. The side chains of Val74 and Leu122 define the surface of the tunnel that is shown in orange. (C) Coarse-graining of hydrogen trajectories inside the enzyme. From the diffusive hopping of H₂ molecules between cavities in the protein, we define clusters centered at the regions of high gas density inside the protein. The clusters are depicted as spheres together with three typical “pathways” to the active site observed by following the trajectories (pathways 1, 2, and 3, colored in red, blue, and yellow, respectively). Cluster E in white is the cluster that gas molecules temporarily occupy before binding; cluster G in gray is the state in which a gas molecule occupies the active site cavity but is not yet chemically bound to Ni. The labels a, b, etc., denote the approximate positions of the Xe-peaks reported in ref 13. Figure adapted from ref. 150 (copyright 2011 American Chemical Society) and 10.

1333 transfer reactions, the proximal [4Fe3S] cluster found in some
 1334 O₂-tolerant [NiFe]-hydrogenases can attain three redox states
 1335 within a redox potential span of only 150 mV (and therefore
 1336 be involved in two-electron transfer reactions), although it is
 1337 unclear if it is a condition for O₂ tolerance¹⁶⁴. The super-
 1338 oxidized state is stabilized by a structural reorganization aris-
 1339 ing from deprotonation of a backbone-nitrogen atom and con-
 1340 comitant nitrogen coordination to one of the iron atoms. X-
 1341 ray diffraction results also suggest that in the enzyme from *E.*
 1342 *coli* a Glu residue is coordinated to Fe2 in the superoxidized
 1343 species (fig. 6), whereas in the membrane-bound hydrogenase
 1344 from *R. eutropha* a dioxygen-derived oxo or hydroxo ligand
 1345 replaces the Glu sidechain¹⁶⁵.

1346 Different spectroscopic techniques (X-ray, EPR, Reso-
 1347 nance Raman and Mössbauer) have been complemented by
 1348 quantum-chemical calculations, with the aim of disclosing
 1349 structural and electronic properties of the unusual [4Fe3S]
 1350 cluster. As an example, broken-symmetry DFT calcula-
 1351 tions complemented Mössbauer measurements, indicating that
 1352 the superoxidized [4Fe3S]⁵⁺ cluster can be described as a
 1353 mixed-valence Fe^{2.5+}/Fe^{2.5+} and a diferric pair. The reduced
 1354 [4Fe3S]³⁺ has an electronic pattern consistent with a mixed-
 1355 valence and a diferrous pair, while the [4Fe3S]⁴⁺ state can be
 1356 described as formed by two mixed-valence pairs. Even though
 1357 these studies agree about the ferric character of the “special”
 1358 Fe ion (Fe2 in fig. 6), the spin coupling scheme of the four Fe
 1359 atoms remains debated. DFT calculations have also been used

to study some aspects of the energetics of the interconversion
 between the three accessible redox states of the [4Fe3S] clus-
 ter^{156,166}.

Many mutations of amino acids near the proximal or medial
 cluster increase the O₂-sensitivity of otherwise O₂-tolerant
 [NiFe]-hydrogenases^{164,165,167}, and it is still unknown how
 the properties of the electron transfer chain make O₂-resistant
 [NiFe]-hydrogenases form, upon oxidation, only a NiB state
 that reactivates very quickly. Certain single point mutations in
D. fructosovorans [NiFe]-hydrogenase also strongly affect the
 rates of anaerobic formation and reactivation of the NiB state,
 for reasons that still need to be clarified. Forty years after
 the NiA and NiB inactive states were discovered, we still need
 to elucidate their structures and mechanisms of formation, not
 forgetting that different mechanisms may operate under oxi-
 dizing aerobic and anaerobic conditions, and lead to the same
 inactive states⁶³. In this respect, it is remarkable that the ac-
 tual reaction of [NiFe]-hydrogenases with O₂ has not yet been
 studied computationally; this is certainly a subject for further
 studies.

4.1.2 Intramolecular diffusion in [NiFe]-hydrogenase

The existence of a gas channel in [NiFe]-hydrogenase was
 recognized when a 2.54 Å resolution structure of the en-
 zyme revealed the presence of hydrophobic cavities connect-
 ing the molecular surface to the active site. A crystallographic

analysis of xenon binding, together with molecular dynamics simulations of xenon and H₂ diffusion in the enzyme, suggested that these cavities were functional¹³. Comparison of amino acid sequences showed that a bottleneck at the end of this channel, near the active site, is shaped by two conserved residues, Val74 and Leu122 (*D. fructosovorans* numbering)¹⁶⁸ (figure 7B), and several subsequent studies suggested that the side chains of these amino acids could influence H₂ and/or O₂ access to the active site^{169–171}.

The suggestion that bulky side chains at these positions may render certain [NiFe]-hydrogenases O₂-resistant by preventing O₂ access, which eventually proved wrong¹⁰, was the initial motivation for a series of studies aimed at determining the effects of amino-acid substitutions in the channel on the functional properties of the enzyme: rates of CO binding, CO release and O₂ binding, Michaelis constant for H₂, and catalytic “bias” (defined as the ratio of the maximal rates of H₂ oxidation and production⁶³). Some results are shown in fig. 8, each data point corresponding to one particular mutant of the [NiFe]-hydrogenase from *D. fructosovorans*. The mutations of amino acids in the channel change the rates of CO binding by up to a factor of 1000, but most mutations have no significant effect on the dissociation constant for CO (fig. 8A shows that k_{out} is proportional to k_{in} in this series of mutants, except for the V74Q, E and N substitutions). The comparison of the rates of reaction with CO and O₂ in this series of mutants (fig. 8B) shows that CO inhibits the WT enzyme and most mutants much more quickly than does O₂, but in mutants where the diffusion is the slowest, the values of k_{in} for O₂ and CO are equal (line “ $y = x$ ” in panel B). This led to the conclusion that CO and O₂ diffuse within the enzyme at the same rate, but O₂ reacts slowly at the active site, suggesting that the rate of inhibition by CO is mainly determined by diffusion towards the active site:

$$k_{\text{in}}^{\text{CO}} = k_1^{\text{CO}} \quad (33)$$

Molecular dynamics simulations of gas diffusion in [NiFe]-hydrogenases gave important clues about the molecular mechanism of inhibitor transport in some of the wild type and mutant enzymes studied experimentally^{150–152}. Before we describe the main findings of the MD simulations, we would like to comment first on the accuracy that one can expect from the molecular models that were used in these simulations.

A good test to assess the force field used to describe the interactions between ligands and proteins is the calculation of diffusion constants in various solvents. The force field models used typically reproduce the lowest non-vanishing multipole moment of the ligands in the gas phase and contain Lennard-Jones interactions sites^{150,151,153}. The solvent is described with the same force field as that used for the protein. Diffusion constants computed for H₂, O₂, CO and CO₂ are summarized in fig. 9 (data taken from ref. 150,151,153). The experimental

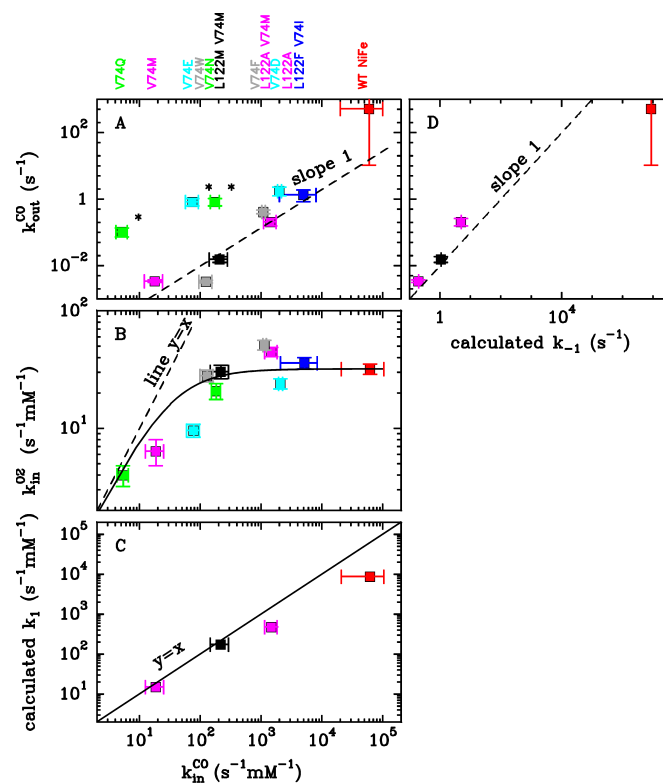


Fig. 8 Summary of the measured and calculated rates of CO binding and release in a series of [NiFe]-hydrogenase mutants where the conserved Val and Leu residues that shape the gas channel have been substituted (fig. 7B). Each data point corresponds to one mutant. The panels show the relations between the experimental values of K_m , $k_{\text{in}}^{\text{CO}}$, $k_{\text{out}}^{\text{CO}}$, $k_{\text{in}}^{\text{O}_2}$, and calculated k_1^{CO} and k_{-1}^{CO} . Data from ref. 10 and 151,152

values are very well reproduced, albeit not perfectly, with a mean relative unsigned error (MRUE) of 15% for water and 21% for hydrocarbons, where the average was taken over the four gases. For O₂, additional calculations were carried out for aprotic dipolar solvents (DMSO, acetone, acetonitrile) resulting in a MRUE of 16%. While there is certainly room for further improvements, the results show that the performance of these simple and computationally efficient force field models is fair.

Regarding intramolecular transport in hydrogenase, the advantage of studying CO over e.g. O₂ is that CO chemical attachment to the [NiFe] active site is fast ($k_2^{\text{CO}} \gg k_{-1}^{\text{CO}}$). Therefore, the bimolecular CO binding rate is a good proxy of the diffusion rate (eq. 33), which allows for a direct comparison between simulated rates for gas diffusion and experimentally determined rates. The diffusion rates of CO in [NiFe]-hydrogenase and three mutant enzymes have been computed using the methodology described in section 2. The results are summarized in fig 8C and D (data taken from ref. 151,152).

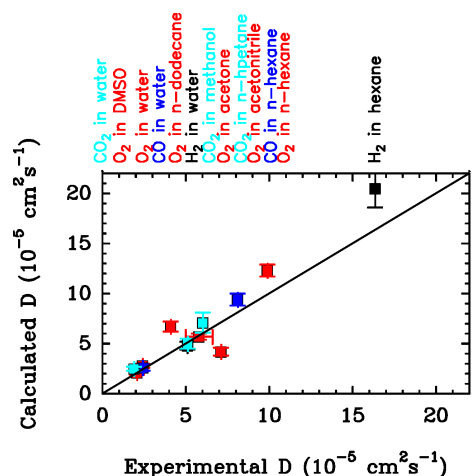


Fig. 9 Computed versus experimental diffusion coefficients for diffusion of H₂, O₂, CO and CO₂ in solvents of different polarity. Calculated values were obtained from MD simulation and taken from ref. 150–153. Experimental data were taken from ref. 172–177.

The simulated rate constants for diffusion in the active site, k_1 , are very close to the experimental binding rate constants k_{in} . They range from $\approx 10^4 \text{ s}^{-1} \text{ mM}^{-1}$ for the WT enzyme down to $\approx 10 \text{ s}^{-1} \text{ mM}^{-1}$ for the V74M mutant (fig. 8D). The very good agreement obtained in this specific case, with deviations of no more than a factor of 3 in the diffusion rates, can be considered somewhat fortuitous given the imperfections of the force field and the statistical errors due to limited sampling. However, a good order of magnitude estimate for the diffusion rate can be generally expected by such simulations. Panel D shows the experimental value of k_{out}^{CO} against the calculated value of k_{-1} , which can be interpreted using eq. 26. The observation that the data points fall reasonably well on a line of slope 1 in a log-log plot shows that the measured value of k_{out} is indeed proportional to the calculated value of k_{-1}^{CO} . We deduce $K_2^{CO} \approx 10^{-2}$, consistent with the approximation made to derive eq. 25. Overall, regarding the kinetics of CO binding and release, the agreement between the model and the data can be taken as an indication that the assumptions underlying the model for gas diffusion developed in section 2 are sound.

We now discuss the measurements and values of dissociation constants^{150,151}. According to both experimental results and computations, CO and O₂ diffuse about equally fast to the active site of [NiFe]-hydrogenase. Every 100 microseconds a CO or O₂ molecule reaches the active site at a gas concentration of the surrounding solution of 1 mM (corresponding to a gas pressure of about 1 atm.). Conversely, it takes only about 100 ns for a gas molecule to diffuse from the active site to the solution. Interestingly, the same time scales have been reported for CO diffusion in myoglobin and for

CO₂ diffusion in ACS/CODH. To first approximation K_1 can be estimated by the ratio of volume per gas molecule in the active site cavity and in solution (since, as explained in ref. 151, the values of K_1 are mainly a consequence of the loss of translational entropy as the ligand moves from the solution to the active site cavity). For more quantitative estimates and to understand differences between ligands, MD simulations must be used to account for specific interactions with the solvent/protein. The calculated equilibrium constant for pure ligand diffusion in [NiFe]-hydrogenase obtained from MD simulations is $K_1 = k_{-1}/k_1 \approx 10^3 \text{ mM}$, and this value is very similar for H₂, CO and O₂.

All experimental mutations studies have focused on the V74 L122 motif and indeed it was unequivocally shown that this motif is one of the bottlenecks for gas transport^{149,152}. However, some of the observed effects were difficult to rationalize. For instance, there was an absence of correlation between the diffusion rate and the “width” of bottleneck shaped by the 74–122 motif. For example, diffusion in the V74M L122A mutant is slowed by a factor of 42 relative to the WT enzyme, even though the gas channel diameter is not significantly reduced¹³⁵. Another puzzling observation is that the L122M V74M double mutation is less effective than the V74M single mutation even though the gas channel diameter is similar to the one for the single mutant according to the crystal structure. Simulations have shown that diffusion is in fact controlled by two rather than one motif, one between residues 74 and 476 and the other between residues 74 and 122¹⁵². The existence of two control points in different locations explains why the reduction in the experimental diffusion rate does not simply correlate with the width of the main gas channel measured between L122 and V74. The simulations also helped us understand how inhibitors can access the active site in certain mutants, despite the fact that the access route is blocked according to the crystal structure¹⁵². Considering one of the most effective mutants (V74M), we found that CO molecules reach the active site due to strong thermal fluctuations of the width of the gas channel defined by M74 and L122 and through transitions that are gated by the microsecond dihedral motions of the side chain of a strictly conserved arginine (R476). These findings suggest that attempts to further decrease inhibitor diffusion could focus on making the main gas channel, in particular the two above mentioned motifs, more rigid.

4.2 Substrate transport in ACS/CODH

Gas diffusion is also a key aspect of the reactivity of bifunctional ACS/CODH (fig. 2C), where structural features allow for the effective transport of substrate and product molecules. In this enzyme, CO₂ diffuses from the solvent to the C cluster located deep inside the protein interior, approximately 30 Å from the protein surface. The reaction product CO is then

transported from the C cluster to the catalytic A cluster of ACS, that is about 70 Å away. Early experimental studies demonstrated that this transport occurs without CO being released to the solvent^{178,179}. More recent xenon-binding studies and calculations of cavities in the static structure^{180–182} showed that the clusters are interconnected by a channel which extends throughout the entire length of the enzyme complex (138 Å). Mutations of putative channel residues resulted in decreased acetyl-CoA production rates, providing convincing evidence that CO molecules use this tunnel¹⁸³.

On a first view, it is puzzling that directional transport of this ligand is possible considering the thermal fluctuations of the protein and the high mobility of the small CO ligand. Why doesn't CO merely take the same route out of the protein as the one CO₂ takes to reach the C cluster from the solvent? After all, CO is smaller than CO₂ and the path that CO₂ takes to diffuse from the solvent to the C cluster should also be accessible for diffusion of CO from the C cluster to the solvent. Molecular dynamics simulations answered this question¹⁵³. It was shown that the hydrogen bonding network in the active site pocket accommodating the C cluster changes drastically with oxidation state. After formation of CO from CO₂, the hydrogen bond network becomes stronger, preventing CO from taking the CO₂ access pathway. Hence, the change in the hydrogen bond network leads to obstruction of the CO₂ channel and enables the directional flow of CO from the C cluster, where it is produced, to the A cluster of ACS/CODH, where it is utilized.

Another puzzling question is how CO₂ diffuses from the solvent to the C cluster of ACS/CODH. Neither Xe-binding studies nor cavity calculations have given indications for a pathway connecting the C cluster and the protein surface¹⁸². Volbeda *et al.* hypothesized that CO₂ could enter the enzyme via the A cluster and travel “backward” through the long CO channel¹⁸⁴. However, the mutations of channel residues do not affect CODH enzymatic activity¹⁸³, and CO₂ transport against CO flux in the channel would require an elaborate mechanism in order to avoid unproductive molecular collisions¹⁸⁴. Tan *et al.* suggested that CO₂ might enter the C cluster through a channel connecting the two C clusters, as shown in cavity calculation, or via a hydrophobic channel near the CODH dimer interface¹⁸⁵. Finally, Doukov *et al.* proposed that the CO₂ diffusion path is dynamically formed by the thermal motion of the protein¹⁸². Recent MD simulations confirmed that CO₂ diffusion into the C cluster is facilitated by a dynamical gas channel that extends orthogonal to the static channel where Xe binds¹⁵³. The cavities of this dynamic tunnel that are close to the active site are temporarily created by protein fluctuations, and as such not apparent in available crystal structures.

With regard to binding kinetics, the experimental information is scarce. Kumar *et al.* determined a rate constant of

$2.6 \times 10^4 \text{ s}^{-1} \text{ mM}^{-1}$ for the CO driven conversion of C_{red1} into C_{red2} at 300 K (calculated from the data measured at 5°C)¹⁸⁶, which provides a lower limit for the rate of diffusion of CO to the active site. One can expect that the rate is lower for CO₂ due to its larger size. The MD simulations that revealed the dynamic access channel (see above) predicted rates of $k_1 = 4800 \text{ s}^{-1} \text{ mM}(\text{CO}_2)^{-1}$ for the diffusion of CO₂ from the solvent to the C cluster and $k_{-1} = 1.5 \times 10^7 \text{ s}^{-1}$ for escape from the C cluster to the solvent¹⁵³. Interestingly, these rates are on the same order of magnitude as those reported for CO and O₂ diffusion in [NiFe]-hydrogenase (see above). Combining the MD simulations with the DFT calculations for CO₂ binding to the C_{red2} state of ACS/CODH, binding rates of $k_{\text{in}} = 4.4 \text{ s}^{-1} \text{ mM}^{-1}$ have been estimated, similar in magnitude to the experimental turnover rate of the enzyme, $k_{\text{cat}} = 1.3 \text{ s}^{-1}$ ¹⁵³. It is interesting to note that the rates for diffusion (k_1) and for chemical attachment (k_2) are very similar, but k_{in} is 3–4 orders of magnitude smaller than both k_1 and k_2 . This can be easily understood when considering the steady-state expression, eq. 21. Since diffusion out of the protein is much faster than chemical attachment ($k_{-1} \gg k_2$), k_{in} is given by k_2 divided by the equilibrium constant $K_1 = 10^3 - 10^4 \text{ mM}$.

4.3 Transformations of the H cluster of [FeFe]-hydrogenase

Several combined electrochemical and DFT studies have been carried out with the aim of characterizing the reactivity of [FeFe]-hydrogenases (fig. 10), even if the quantitative comparison of rate and binding constants obtained using PFV and chronoamperometry experiments with the corresponding computed data can be problematic, due to the limited accuracy of present DFT methods (see sections 1 and 2).

4.3.1 Inhibition by formaldehyde

Recently, Armstrong and collaborators observed that formaldehyde reversibly inhibits [FeFe]-hydrogenase by targeting the reduced H cluster. DFT calculations were carried out with the aim of characterizing the species formed when the enzyme reacts with the H cluster in the Hox state, or its one- or two-electron reduced forms Hox₋₁ and Hox₋₂, respectively¹⁸⁸ (fig. 10). Two possible reaction mechanisms were evaluated: (a) nucleophilic attack of a Fe_d hydride species at the carbonyl group of HCOH and (b) Schiff base chemistry involving the bridgehead N atom of the dithiolate chelating ligand. Considering the hydridic reaction with HCHO at the Hox₋₁ redox level, the formation of methanol bound to Fe_d via the oxygen atom is strongly exothermic ($\Delta E = -28 \text{ kcal/mol}$, the resulting species is labelled “Hox₋₁(f)” in fig. 10). The Hox₋₁ state of the H cluster is therefore thermodynamically competent to bind

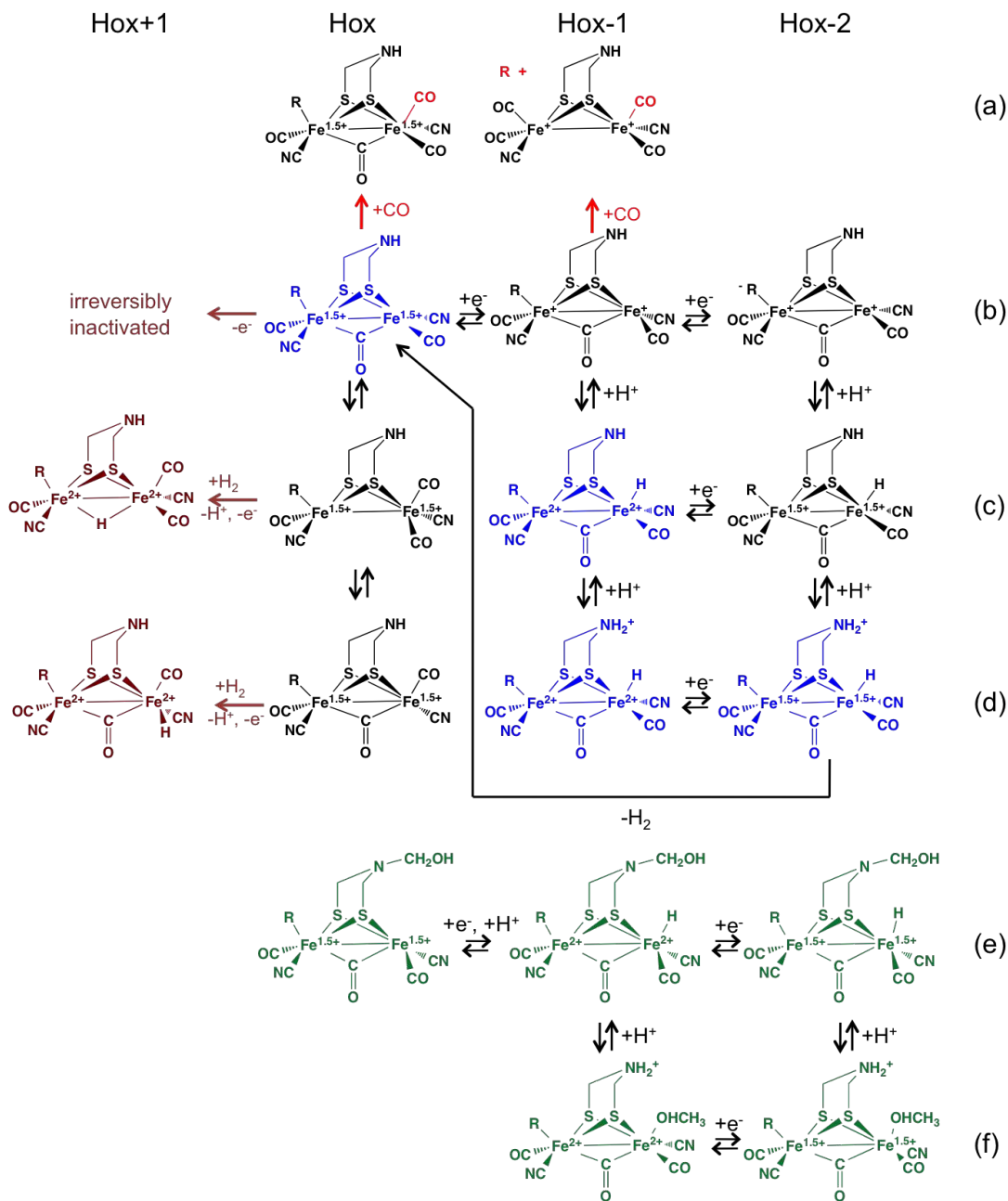


Fig. 10 Proposed chemical transformations of the H cluster of hydrogenase, which occur when the enzyme reacts with CO (red)¹⁸⁷, formaldehyde (in green)¹⁸⁸ and under oxidizing conditions in the presence of H₂ (ref. 8). The structures in blue are believed to be part of the catalytic cycle. “R” represents the [4Fe4S] subcluster. The catalytic relevance of the “super-red” species “Hox₂(b)”, where the [4Fe4S] subsite of the H cluster is reduced, is unclear^{7,189}.

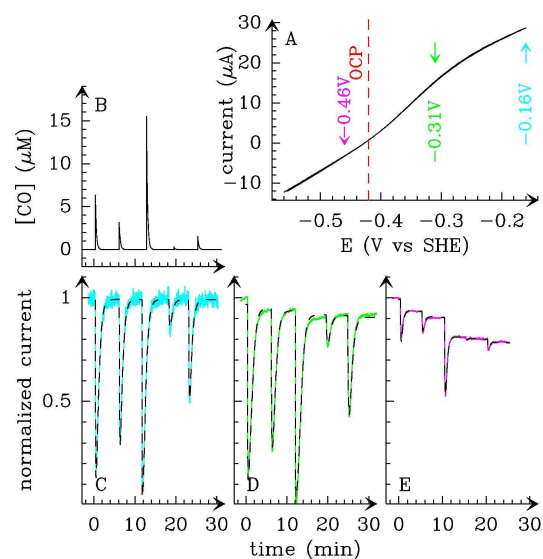


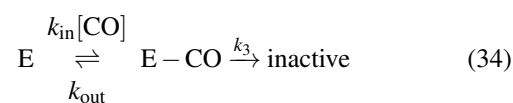
Fig. 11 (A) Steady-state voltammogram for *Ca* [FeFe] hydrogenase. The open circuit potential (OCP) is indicated by a dashed red line. (B) CO concentration against time. (C-E) Normalized current traces showing the activity changes that result from the sequence of injections shown in panel B, recorded at $E = -0.16$ (C), -0.36 (D), and -0.47 V (E). The dashed lines are the best fit to the model based on eq. 34. From ref. 187, copyright 2011 Americal Chemical Society.

HCHO. Further addition of an electron slightly increases the exothermicity of the reaction ($\Delta E = -34$ kcal/mol). DFT calculations also suggested that the reaction of HCOH with the bridgehead N atom of the dithiolate chelating ligand could yield aminol intermediates (Hox(e), Hox₋₁(e) and Hox₋₂(e) in fig. 10, reaction energies $\Delta E = -18$, -17 , and -22 kcal/mol, respectively), which are expected to decompose in a protic environment to yield dehydrated imine species.

This investigation illustrated how the combined used of PFE and DFT allowed to evaluate plausible reaction pathways for the reactivity of [FeFe]-hydrogenases with HCOH, but also highlighted intrinsic limitations in these approaches. In particular, even if both the formation of a strongly bound methanol molecule and a Schiff base modification of the H cluster are consistent with the enzyme inhibition observed when H₂ production is monitored at very negative potentials, these scenario are necessarily incomplete since they do not account for the observed reversibility of the inhibition process, leading the authors to conclude that the protein environment around the H cluster may play an important role in destabilizing or hindering the formation of the predicted products.

4.3.2 Inhibition by exogenous CO

The role of the protein surrounding the H cluster was clearly highlighted in a recent combined experimental and theoretical study of the reaction of extrinsic CO with the H cluster of [FeFe]-hydrogenase¹⁸⁷. CO behaves as a mere competitive inhibitor when the enzyme is inhibited under very oxidizing conditions (leading to Hox(a) in fig. 10); in other conditions, the reaction with CO is partly irreversible^{136,187}, as illustrated in fig. 11. These experiments are the same as those described to study CO binding to [NiFe]-hydrogenase in fig 5, but here the observation that the activity is not completely recovered after CO is flushed away reveals an irreversible process. The data could be accurately analyzed in ref 187 using a model that assumes that the inactive enzyme-CO complex can either dissociate or be transformed irreversibly into an inactive form.



The rate of CO binding depends on electrode potential in a sigmoidal manner, with a mid-point potential that appears to match the value expected for the Hox/Hred transition. The change in rate of irreversible transformation of the enzyme-CO complex and the change in k_{in} occur at the same potential, which suggested that the Hred state is irreversibly degraded after it binds CO. DFT was used to carry out geometry optimization of the partially oxidized and one-electron reduced forms of the H cluster bound to exogenous CO (such enzyme forms are termed Hox-CO and Hred-CO in the following). The experimental free energy of formation of Hox-CO, deduced from the ratio of k_{out} over k_{in} , is reasonably reproduced by calculation (see also ref. 190), although it must be noted that the ± 2 kcal/mol uncertainty in the calculated value corresponds to a large difference in terms of K_d , a factor of 800. The calculations showed that in Hox-CO, the H cluster is stable, while in the case of Hred-CO, the Fe_p-S(Cys) bond that covalently attaches the diiron cluster to the enzyme is cleaved (leading to Hox₋₁(a) in Figure 10). This behaviour can be qualitatively rationalized simply by using electron count rules: in Hred, the iron atoms already have 18 valence electrons, a configuration which is particularly stable; upon coordination of an additional CO ligand, the weakest bond (the Fe_p-S(Cys) bond according to DFT) has to be cleaved if the 18-electron rule is still to be fulfilled. The resulting $[\text{Fe}_2(\mu\text{-SR})_2(\text{CO})_4(\text{CN})_2]^{2-}$ complex is a stable species, which explains why the reaction of Hred with CO is partly irreversible. Following bond rupture, the fate of the diiron subcluster should depend on the surrounding protein matrix, and Baffert and coworkers considered as unlikely that the diiron site is released from the protein because the H cluster is deeply buried and shielded from the solvent.¹⁸⁷

The reverse reaction, that is, transfer of $[\text{Fe}_2(\mu\text{-SR})_2(\text{CO})_4(\text{CN})_2]^{2-}$ (a 2Fe(I) precursor of the diiron subsite) from the solvent to the active site pocket of an apo form of [FeFe]-hydrogenase, has recently been observed by Happe and collaborators^{16,191}. This implies that the organometallic complex is able to autonomously integrate into the protein core, and to covalently bind the [4Fe4S] subsite with concomitant release of one carbonyl ligand. However, it is believed that insertion of the 2Fe subcluster occurs through a cationically charged channel that collapses following incorporation¹⁹².

4.3.3 Inhibition by dioxygen

As mentioned above, a topic of increasing relevance in the hydrogenases field concerns the reactivity of these enzymes towards molecular oxygen. From the results of electrochemical measurements with the [FeFe]-hydrogenases from *C. acetobutylicum*, Baffert and coworkers proposed that the aerobic inactivation of the enzyme occurs as a result of initial, slow and reversible formation of an O_2 adduct, followed by an irreversible transformation; when the reaction is monitored by following the change in catalytic current caused by a pulse of O_2 , the kinetic scheme that can be used to analyse the data and measure the rate constants of the three reactions is the same as that considered above for CO binding (eq 34)^{10,193}. That O_2 initially targets the distal Fe of the 2Fe subsite is clear from the observation that the competitive inhibitor CO binds on this atom in the crystal¹⁹⁴ and protects the enzyme from O_2 inactivation^{193,195}.

This is consistent with the theoretical investigation by Stiebritz and Reiher, who used DFT to examine the regioselectivity of O_2 binding^{196,197}. A subsequent study by Hong and Pachter, based on both MD simulations and DFT calculations, corroborated such picture.¹⁹⁸ Blumberger and coworkers investigated the kinetics of the initial O_2 binding step using DFT calculations¹⁹⁹: by parametrizing a range-separated density functional using high-level ab initio data as a benchmark, they could compute an activation free energy barrier of 13 kcal/mol for O_2 attachment to Fe_d , and a binding free energy of -5 to -7 kcal/mol. The rate of O_2 binding could then be calculated from eq 21 above. Converting the computed free energies into k_2 using TST and adopting values for k_1 and k_{-1} from MD simulations for [NiFe]-hydrogenase, they obtained values for k_{in} of $3.6 \text{ s}^{-1}\text{mM}^{-1}$ and $1.2 \text{ s}^{-1}\text{mM}^{-1}$ for *Cp* and *Dd* enzymes, respectively, in fair agreement with the experimental values ($2.5 \text{ s}^{-1}\text{mM}^{-1}$ and $40 \text{ s}^{-1}\text{mM}^{-1}$, respectively¹⁰). The reason the kinetics of O_2 binding and release is different in the three homologous [FeFe]-hydrogenases for which such data have been published^{10,136,193} remains to be clarified.

In contrast with the above experimental and theoretical evi-

dence that O_2 targets the distal Fe on the 2Fe subcluster, X-ray absorption measurements indicated that the main structural consequence of the exposure to O_2 is oxidative damage of the [4Fe4S] subcluster¹⁹⁵. Armstrong and coworkers concluded that the destruction of the 4Fe subcluster follows up O_2 binding at the catalytic site of [FeFe]-hydrogenase and proposed two mechanistic scenarios: (i) the formation of a reactive oxygen species (ROS) that diffuses towards the [4Fe4S] subcluster and destroys it, or (ii) long-range damaging effects on the same iron-sulfur site exerted by an O_2 -derived superoxide ligand stably bound to Fe_d . Happe and collaborators²⁰⁰ ruled out the latter hypothesis by monitoring the time evolution of the X-ray absorption spectra of *Cr* [FeFe]-hydrogenase exposed to O_2 . Three kinetic phases could be distinguished. A fast oxygenation phase (faster than 4 s) is characterized by the formation of an increased number of Fe-CO bonds, elongation of the Fe-Fe distance in the binuclear subcluster, and oxidation of one iron ion; the subsequent inactivation phase (≈ 15 s) causes a 50% decrease of the number of 2.7 Å Fe-Fe distances in the [4Fe4S] subcluster and the oxidation of one more iron ion. The final, degradation phase (< 1000 s) leads to the disappearance of most Fe-Fe and Fe-S interactions and further iron oxidation. A DFT study again by Reiher and coworkers²⁰¹ evidenced that the O_2 -derived species most likely involved in the degradation of the [4Fe4S] subcluster are the OOH radical and H_2O_2 : the direct coordination of the former on the Fe atoms of the cubane is favored, whereas H_2O_2 reacts more easily with the cysteinyl sulfur ligands of the H cluster model.

In any case, all studies agree about the initial step of O_2 attack, and this is relevant to the engineering of [FeFe]-hydrogenase that are more resistant to O_2 . In particular, based on the observation that electron transfer from the di-iron subsite to O_2 makes oxygen attachment thermodynamically favorable, Blumberger and coworkers proposed that mutations that counteract this electron transfer may help to increase oxygen resistance¹⁹⁹. This working hypothesis should now be tested by characterizing the kinetics of inhibition of these mutants.

Taken as a whole, the above results raise hopes that the dialogue between theory and experiments in this challenging case of protein engineering will provide even more fruitful outcomes in the near future.

4.3.4 Flexibility of the H cluster

In a very recent contribution of ours⁸, electrochemistry was combined with site directed mutagenesis and quantum and classical calculations to dissect the steps leading to oxidative inactivation of [FeFe]-hydrogenases and learn about the binding of H_2 to the active site of [FeFe]-hydrogenase. By discussing in details hereafter the path that led us to the proposed mechanism, we intend to illustrate the potential synergy in combining computational and experimental approaches.

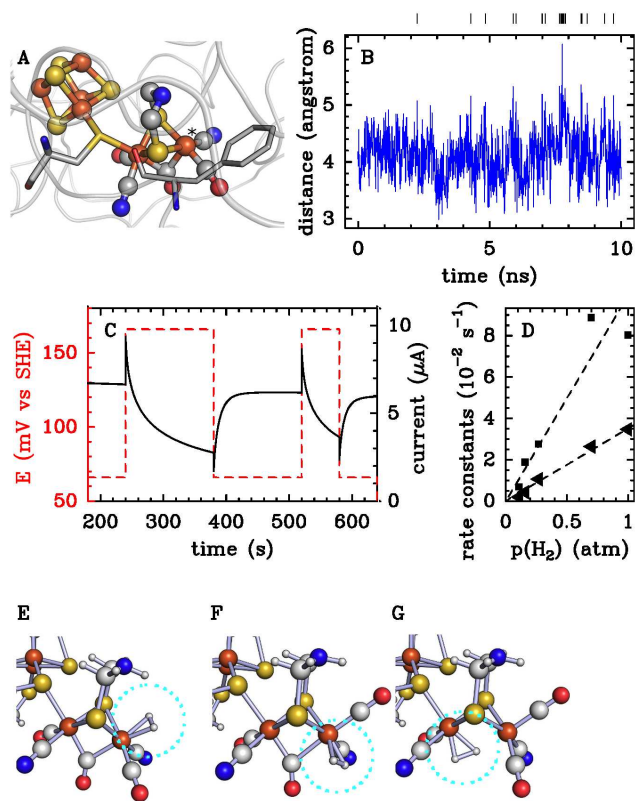


Fig. 12 Investigation of the mechanism of oxidative inactivation of [FeFe]-hydrogenase. (A): The active site H cluster of [FeFe] hydrogenases, and its surroundings (adapted from PDB 3C8Y)²⁰². The vacant coordination position on the distal iron is marked by an asterisk. The phenylalanine residue is discussed in the text. (B): Results from MD calculations: thermal fluctuations of the distance between the distal Fe atom of the H cluster (Fe_d) and the $\delta 2\text{C}$ atom of Phe as a function of simulation time. The vertical lines show the moments when the distance is greater than 5 Å. (C): Electrochemical study. Sequence of potential steps applied to the electrode (red) and the resulting catalytic current (black). (D): Dependence of inactivation rate constants (measured from data such as those in panel C) on H_2 partial pressure. (E-G): Results of DFT calculations. (E): Structures of the “normal” H_2 adduct. (F) and (G): Structures of the two inactive adducts. Adapted from ref. 8.

The key issue in this study was to rationalize the occurrence of different intermediates formed when [FeFe]-hydrogenase are oxidized in the presence of H_2 . Spectroscopy is difficult to use in this context, since turnover prevents equilibrium from being reached under these conditions, but a redox titration of the enzyme from *C. reinhardtii* followed by FTIR showed that full oxidation in the absence of H_2 destroys the H cluster⁴⁴, and PFV experiments demonstrated that if H_2 is present, the enzyme inactivates reversibly (at least partly reversibly) at high potential²⁰³.

Previous experiments on bio-inspired model complexes²⁰⁴ suggested that oxidation of Hox prior to H_2 binding could trigger coordination of the pendant amine in the H cluster to the distal iron atom (Fe_d); formation of such bond would inactivate the enzyme by preventing H_2 binding to Fe_d . We considered an intramolecular reaction of this kind as a first hypothesis for the mechanism of reversible oxidative inactivation, but we had to rule it out based on the results of DFT calculations. Indeed, a small model of the H cluster in overoxidized state did show barrierless formation of $\text{Fe}_d\text{—N}$ bond along geometry optimization, but no such bond is formed when relevant portions of the protein are also included in the model²⁰⁵.

Chronoamperometry experiments can be analysed in a qualitative manner, to observe that the enzyme activates or inactivates, but we have also developed methods for precisely measuring the rates of the transformations in experiments where the electrode potential is repeatedly stepped up and down to trigger (in)activation^{6,206,207}. Analysing experiments such as those in fig 12C, we demonstrated that [FeFe]-hydrogenase undergoes both reversible and irreversible inactivation at high potential. The activity loss, evidenced by a decrease in H_2 oxidation current, is clearly bi-exponential, which we interpret as an evidence that the active species (Hox) reversibly converts into *two* inactive species. Moreover, the dependence on pH of the two rate constants of reactivation of the inactive states indicates that the formation of each inactive species corresponds to a one-electron oxidation of the active site that is coupled to the loss of one proton. This is remarkable because the H cluster has only one acidic proton, on the pendant amine, which should be tightly bound (indeed, DFT calculations suggest that deprotonation leads to the cleavage of one of the C—S bonds within DTMA). Our observation is therefore inconsistent with the former hypothesis that inactivation results from the intramolecular binding of the nitrogen atom of dtma.

In search of the origin of the two protons released upon oxidation, we were tempted to consider that inactivation could result from the binding of a water molecule; indeed, $\text{Fe}_d\text{—OH}_2$ bond formation would make water significantly acid. An oxygen atom bound to Fe_d is present in the models of the crystal structure of *Clostridium pasteurianum* [FeFe]-hydrogenase,^{202,208} but it was difficult to imagine that there could be two isomers of this water complex, whereas the electrochemical data clearly reveal the formation of two distinct, inactive species.

Another ligand whose acidity increases upon metal binding is H_2 . With this idea in mind, we examined the dependence of the reversible inactivation rate constants on H_2 partial pressure; the experimental results in fig. 12D showed that the two rate constants of inactivation are proportional to H_2 concentration, meaning that regarding each of the two inactive species, H_2 binding is actually the first step of the inactivation reac-

tion. This led us to look for three distinct modes of H₂ binding to the H cluster, two of which would be non-productive. Since the only vacant coordination site is on Fe_d, we hypothesized that alternative coordination sites may be created after the movement of the intrinsic CO ligand that is bound to Fe_d to an axial position, and/or the movement of the bridging CO to a terminal position on Fe_d (fig. 10, Hox(b), (c) and (d) isomers); we considered as unlikely that the CN⁻ ligand on Fe_d would move, because it is bound to a conserved lysine residue by a hydrogen bond²⁰⁹. Inspection of the protein crystal structure indicates that the interconversion among the three possible conformers of the H cluster may be impeded by the presence of the bulky side chain of a conserved phenylalanine residue (F234 in *Cr* hydrogenase) shown in fig. 12A. However, molecular dynamics calculations showed that thermal fluctuations of the structure are sufficiently large to allow the movements of iron-bound carbonyl ligands and the isomerisation of the active site (fig. 12B). We used DFT to describe the intermediates involved in the inactivation process. DFT confirmed (through the comparison of reaction energies) that H₂ binding can occur not only on the “normal” binding site (fig. 12E), but also on two minor (i.e. higher in energy) vacant coordination sites (fig. 12F & G). The calculations suggest that the H–H bond is cleaved in all cases (fig. 10), but binding on the abnormal sites leads to species that are essentially inactive, because no base is sufficiently close to the coordinated H₂ molecule to quickly accept the proton that is produced upon heterolytic cleavage.

This mechanism is supported by other experimental findings, such as the effect of replacing phenylalanine with tyrosine (which prevents isomerisation and slows down reversible inactivation), and the fact that the two inactive states are protected against O₂ attack (the coordination sphere of Fe_d is complete when H₂ binds to abnormal positions). The electrochemical data also show that the two H₂-bound oxidized forms are not destroyed at high potential, unlike the fully oxidized H₂-free H cluster (Hox₊₁(b) in fig. 10); this is consistent with the previous observation of Lubitz and coworkers⁴⁴; we therefore hypothesized that the oxidative, irreversible inactivation arises from the attack of the distal Fe_d by a nucleophilic molecule (e.g. water) which competes with H₂ binding.

Overall, this is a case where all experiments and calculations converge on the conclusion that the H cluster is more flexible, and its chemistry more versatile, than had been anticipated based on the crystal structure. This may be relevant in the case of other inorganic active sites.

4.4 Long range proton transfer (PT)

The catalytic cycles of the redox enzymes that we discuss here involves transfers of protons and electrons over long distances, between the active site and the solvent or the redox

partner. The crystal structures of hydrogenases and CODH immediately give the information about the electron transfer pathways, which is a chain of FeS clusters. However, experimental information about the kinetics of elementary ET steps along this chain is scarce^{127,213}, and calculations of ET rates virtually non-existent (this contrasts with the situation where hemes mediate long range electron transfer^{84,214–219}).

In contrast, the path taken by protons cannot always be deduced from the X-ray structure in a straightforward manner, and calculations by different authors sometimes give different results (in the case of [NiFe]-hydrogenase, the PT pathway is still elusive). Measuring the rate of PT in an enzyme is straightforward only if PT is the rate limiting step, as occurs with carbonic anhydrase. Using site-directed mutagenesis to identify a PT pathway may prove particularly challenging, as illustrated below.

4.4.1 [FeFe]-hydrogenases

Based on the initial structure of the enzyme from *C. pasteurianum*, Peters and coll. suggested that Cys299 could act as a proton donor for the formation of dihydrogen, and identified a putative PT pathway connecting the protein surface to C299, involving two Glu residues, a Ser residue, and a water molecule,²⁰⁸ as shown in fig. 13A. This pathway has been widely supported by calculations^{220–223} and site-directed mutagenesis studies^{224,225}.

Hong and collaborators²²⁰ used a combination of DFT and QM/MM molecular dynamics simulations to study plausible PT pathways from the enzyme surface to the H cluster. Although free energies were not computed and therefore this study provided only qualitative information, the results are consistent with experimental evidences, and suggest a mechanism in which protons move from E282 to E279 via S319 and from E279 to C299 via water612. Ginovska-Pangovska *et al.*²²¹ carried out a series of classical MD simulations in the wild type enzyme, as well as in a series of mutants, starting from the assumption that a well-defined and stable hydrogen bonding network is fundamental for efficient PT. Their results also support the pathway shown in fig. 13A and suggest the existence of a persistent hydrogen bonded core (residues C299 to S319), with less persistent hydrogen bonds at the ends of the pathway for both H₂ release and H₂ uptake. Long *et al.*²²² combined classical MD simulations, free energy perturbation and QM/MM calculations to quantitatively investigate the kinetics and thermodynamics of the PT pathway described by Hong and collaborators²²⁰. It turned out that the side chains of E279 and E282 could adopt two different conformations, depending on their protonation state, and are well suited to play the role of proton shuttles. In particular, a proton from bulk water can enter the protein through E282, and then be transferred to C299 via pathways that involve E279 and S319.

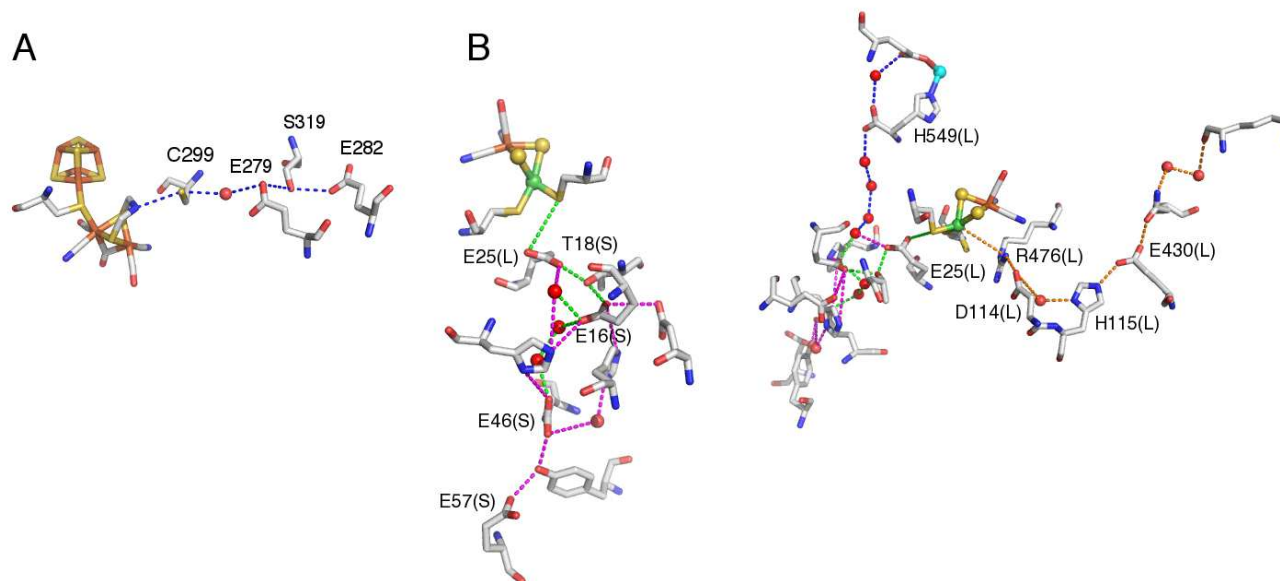


Fig. 13 Putative proton transfer pathways in [FeFe] (panel A) and [NiFe]- (panel B) hydrogenases. In A, we number the amino acids according to the sequence of *C. Pasteurianum* [FeFe]-hydrogenase (pdb 3C8Y). The equivalent pathway in *D. desulfuricans* [FeFe]-hydrogenase is C178/E156/S198/E159. In B, the letters S and L between brackets are used to indicate that the amino acid is in the small or the large subunit of the dimer, respectively. We show in green and blue the pathways identified by Volbeda and coworkers in ref 210, in purple the pathway proposed by Teixeira *et al.* in ref 211, in orange the pathway proposed by Carrondo *et al.* in ref 212.

The importance of S319 and C299 was supported by running calculations with *in silico* mutants: according to the analysis of the QM/MM MD simulation trajectories, the S319A and C299S mutations prevent PT during the simulation time²²⁰. The effect of single substitutions (C299S, E279D and E282D) has also been assessed *in silico* by examining the disruption in the hydrogen bonding network.²²¹

The C299S mutant is indeed inactive in H₂ evolution according to three independent investigations^{224–226}. The enzyme retains activity only when C299 is replaced by aspartic acid²²⁶. It has been observed that the C299A, C299S, E279D, E279L and S319A mutants have no H₂ evolution activity, but 5 to 30% residual H₂ oxidation activity, whereas the E282D and E282L mutants have 5–30% residual activity in both directions.²²⁴ The authors rule out the relevance of a second putative PT pathway starting from C299, passing through several modelled water molecules and S298, and ending at the non-conserved K571 residue at the enzyme surface by showing that S298 is not critical for activity (the S298A mutation has no effect).

4.4.2 [NiFe]-hydrogenase

The situation is far less consensual in the case of [NiFe]-hydrogenases; this example illustrates the limitations of both

the experimental and theoretical methods for studying the kinetics of PT in complex enzymes, and the difficulty in combining the information in that case. Many distinct PT pathways have been proposed based on the examination of the X-ray structures of the [NiFe] enzymes from *Desulfovibrio* species^{45,212,227}, *E. coli*²²⁸ and *Hydrogenovibrio marinus*¹⁵⁴. Figure 13B only shows those that have been selected in computational studies^{210–212}. According to these results, PT to/from the active site occurs either between the sulfur atom of a cysteine ligand to the Ni and E25 of the large subunit, or between the Ni and R476 of the large subunit (*D. fructosovorans* numbering). Both amino acids are fully conserved. In this section, we indicate by (L) or (S) the location of the amino acids in the large or small subunit of the enzyme.

On the basis of calculations, and assuming E25(L) as the starting point, complete pathways have been proposed (fig. 13B), using structures of enzymes from *D. fructosovorans*²¹⁰, *D. gigas*²¹¹ and *D. vulgaris*²²⁹. In particular, Baptista and collaborators²¹¹ used a combination of Poisson-Boltzmann and Monte Carlo simulations, as well as a distance-based network analysis, to investigate possible proton pathways in *D. gigas* [NiFe]-hydrogenase, considering different pH values. Poisson-Boltzmann and Monte Carlo techniques were used to compute the pK_a values of protonatable groups within the protein, whereas the distance-based

network analysis was used to find likely pathways for the proton transport. A PT pathway was proposed between the active site and the surface that mainly involves glutamate and histidine residues: E18(L), H20(L), H13(S), E16(S), Y44(S), E46(S), E57(S), E73(S), and some water molecules (purple in fig. 13). Fdez Galván *et al.*²¹⁰ carried out a QM/MM study of the [NiFe]-hydrogenase from *D. fructosovorans*, computing reaction and activation energies for plausible pathways. In this case, the calculations were carried out not only on the crystallographic structure, but also considering several structures of the protein obtained from MD simulations. Higher level quantum chemical (DFT) corrections were also made to some of the calculated energy profiles. The pathway characterized by the most favorable energy profile involves PT via E25(L), E16(S), and E46(S) (green in fig. 13), and corresponds approximatively to the pathway proposed by Teixeira *et al.*. A second pathway (blue in fig. 13), which involves E25(L), H549(L), and E53(L), was characterized by a less favorable reaction energy profile. Notably, Galván *et al.* underlined that the results obtained in their work, as well as in the study by Teixeira *et al.*²¹¹, could not be considered conclusive because only a limited set of possible pathways was examined. In addition, only “static” pathways were considered, not considering possible alternatives forms produced by medium- or large-scale movements of the protein. In a later work, Summer and Voth²²⁹ studied PT in *D. vulgaris* Miyazaki F [NiFe]-hydrogenase using multi-state empirical valence bond (MS-EVB) reactive MD simulations, coupled to an enhanced path sampling methodology. MS-EVB, which is a molecular-mechanics approach that dynamically allows chemical bonds to break and form during MD simulations, was coupled with metadynamics, which can be used to find complex, nonlinear minimum free-energy pathways. In contrast with the previous computational studies, this methodology allowed to find unbiased PT pathways, i.e. without making *a priori* assumptions. Each simulation was initialized with a hydronium near residue E34(L), which is the assumed initial site in the PT chain, and three PT pathways were found. The preferred pathway, as deduced considering the frequency with which this pathway was found in all active site geometries and oxidation states under consideration, is in agreement with previous proposals, and involves H13(S), E16(S), T18(S), H36(L), E46(S), E57(S), and E75(S). Notably, the residues E16(S), T18(S) and E75(S) (E16(S), T18(S), and E73(S) in *D. gigas*) are conserved in the [NiFe]-hydrogenases from all *Desulfovibrio* species.

A completely different pathway starting with R476 of the large subunit has been proposed on the basis of the examination of the structure of *D. desulfuricans* hydrogenase²¹² and recently supported using calculations with the structure of the [NiFe]-enzyme from *D. vulgaris*²³⁰. The observation that the sequences of the large subunits of almost all membrane-bound [NiFe]-hydrogenases shows a highly con-

served histidine-rich region, prompted Kovacs and collaborators²³⁰ to carry out a computational and experimental study on the [NiFe]-hydrogenase from *T. roseopersicina*. Only two of these conserved histidines are present in the cytoplasmic hydrogenase (H104 and H110, in *T. thiocapsa roseopersicina*, H124 and H130 in *D. vulgaris*). Since the structure of the enzyme from *T. roseopersicina* has not yet been determined, and considering that a homology model could not be used to propose possible proton-hopping mechanisms due to the fact that the positions of structural water molecules could not be predicted, the authors analyzed the X-ray structure of the [NiFe]-hydrogenase from *D. vulgaris* Miyazaki F. The protonation state of the aminoacids at pH 7.4 and the preferred orientation of the structural water molecules were predicted minimizing the total free energy of the system. Based on the analysis of networks of hydrogen bonds, it was concluded that, among the conserved His residues, only H104 plays an important role in the enzyme function, suggesting that this residue could be part of an alternative PT route involving R487, H104 and D103.

The above results obtained in the computational investigations highlight peculiar problems connected to the prediction of PT pathways. First of all, it should be noted that to properly model PT in proteins one should not only take into account proton migration between different sites (which is a reactive event), but also consider the dynamics of the protein, and the possible involvement of solvent molecules in the PT chain. The most rigorous approach to study such process in an unbiased way would imply to use QM methods to model both the reactive and dynamical behavior of the system, which is clearly prohibitive. Therefore, in a more realistic way, PT pathways have to be studied using complex *ad hoc* computational schemes, either by postulating *a priori* possible pathways, or without any bias but using a more qualitative level, which necessarily includes some empirical parameters. In this context, the different computational approaches discussed above have been very helpful for the suggestion and evaluation of plausible PT pathways, even if the comparison of results obtained from different methods is challenging.

It is not easier to discriminate between the three main putative pathways in [NiFe]-hydrogenase using site-directed mutagenesis.

The hypothesis that the first PT relay is E25(L) was supported by a site-directed studies, showing that replacing E25 with a non-protonatable glutamine abolishes PT in the enzyme from *D. fructosovorans*²³¹ and the hydrogen-sensor hydrogenase from *Ralstonia eutropha*²³². That the active site is functional in the two E25(L)Q mutants was confirmed by the observation that they retain the ability to convert ortho and para dihydrogen²³³.

In contrast, the relevance of the rightmost pathway in fig 13B is supported by the characterization of site-directed mutants of the enzyme from *T. roseopersicina*: the replacement

of E14 (E25(L) in *D. fructosovorans*) with a glutamine results in only a two-fold decrease of the H₂ oxidation/production rates²³⁰, whereas the D103L, H104A and H104F have little activity (*D. fructosovorans* numbering R476(L), D123(L), H115(L)). The function of arginine shown in fig 13B cannot be tested by site-directed mutagenesis: the attempts to produce the R476K and R476L mutants of *D. fructosovorans* [NiFe]-hydrogenase, and R487I of *T. roseopersicina* hydrogenase failed, the bacteria did not produce a mature form of the enzyme (unpublished results of ours and ref 230). Since the amino acids involved in the two pathways are present in both hydrogenases (*T. roseopersicina* and *D. fructosovorans*) it is unclear how a single pathway can be functional in each enzyme.

Overall, testing the putative PT pathways in hydrogenases and other complex metalloenzymes appears to be very difficult for a number of reasons.

(1) In contrast to the case of carbonic anhydrase discussed below, there is no indication that PT limits the rate of H₂ oxidation, H₂ production or isotope exchange in WT [NiFe]-hydrogenase. This implies that a mutation that decreases slightly or increases the rate of PT may have no apparent effect. There is no experimental method that measures the rate of single PT events in hydrogenases. Any *quantitative* comparison between the computational and experimental characterization of site-directed mutants is therefore impossible.

(2) Unlike electron transfer pathways, the putative PT pathways may be highly ramified. Even the E25(L)-E57(S) pathway depicted in fig. 13B involves many parallel routes. If they were functional, this would imply that several branches of a ramified pathway have to be blocked in a single mutant in order to observe an effect.

(3) Another problem is very general regarding studies based on site-directed mutagenesis: it is not always possible to make sure that substituting an amino acid has no side effects. There are examples in the literature where a mutation intended to interrupt a PT pathway does not have the expected effect because a water molecule is stabilized in the mutant and substitutes for the missing side chain²³⁴.

It may also be that structural rearrangements remote from the site of the mutation disrupt the hydrogen bond network or create new PT pathways. Regarding the works cited in this section, none of the mutants have been crystallized to make sure that such effects are not the cause of the observed phenotypes. The (unpublished) observation of ours that the E46(S)Q mutant of *D. fructosovorans* [NiFe]-hydrogenase has approximately 50% of the WT H₂ oxidation/production rates may suggest that E46(S) is not essential, but only if we can rule out the above mentioned artifacts. In contrast, we have observed that the E16(S)Q and E16(S)V mutations in *D. fructosovorans* [NiFe]-hydrogenase severely affected both H₂ production/oxidation and isotope-exchange activity (unpublished),

but it is not unambiguous evidence that PT is impaired in these mutants.

Worse, a mutation design to assess a PT pathway may also affect steps others than proton transfer. The T18(S) amino acid shown in fig. 13B is next to a cysteine ligand of an electron transfer cluster (C19(S)) and its backbone shapes the substrate gas channel. Replacing T18(S) may affect the activity in a way that is mistakenly interpreted as revealing the disruption of a PT pathway.

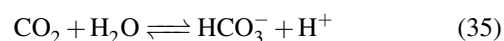
(4) Last, the mutation of a side chain putatively involved in PT sometimes prevents protein folding. We have not been able to replace H549(L), which is a direct ligand of a putative Mg ion (turquoise in fig. 13B) and appears to have a structural role. And we failed to discriminate between the two pathways starting with E25(L) by examining the effect of replacing the E57(S) and H549(L) residues, because the mutants we constructed could not be produced (E57Q, H549R, H549Q, H549V in *D. fructosovorans* [NiFe]-hydrogenase; unpublished results).

Overall, regarding PT in hydrogenases, we must acknowledge that rather limited results have been achieved since it became possible (in the late 1990's) to use site directed mutagenesis to test the numerous putative pathways detected in the crystal structures. This is because there is no direct measurement of the rate of PT in hydrogenase, and no strong conclusion about the effect of a mutation can be reached if the mutant of interest is not fully characterized using crystallography, spectroscopy, kinetic methods, etc.

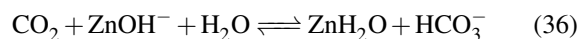
4.4.3 PT in carbonic anhydrase

Carbonic anhydrase is one of the rare enzymes in which the chemical step of catalysis is so fast that intramolecular PT is rate limiting, which allows this transfer to be studied in detail.

The mammalian enzyme carbonic anhydrase II (CAII) catalyses CO₂ hydration into HCO₃⁻ and the reverse reaction, which are involved in various physiological processes:



The active site is a Zn centre coordinated by three His nitrogen atoms and one OH⁻ ligand. The catalytic cycle includes a chemical step:



and the transfer of the extra proton to a buffer base B through His64 :



The maximum turnover rate of CAII is 10^6 s^{-1} for the hydration reaction and $5 \times 10^5 \text{ s}^{-1}$ for the inverse reaction, which makes this reaction one of the fastest catalyzed reactions. Both rate constants were shown to decrease four-fold when the reactions took place in D_2O and it was soon demonstrated that intramolecular PT (reaction 37a) is rate limiting. The activation free energy deduced from the temperature dependence of the catalytic constant of the hydration reaction is $\Delta G^\ddagger = 9.0 \text{ kcal/mol}$ at 25°C . Carbonic anhydrase is one of the rare enzymes in which the chemical step of catalysis is so fast that intramolecular PT is rate limiting, which allows this transfer to be studied in detail. Several mutated forms of the enzyme were prepared to elucidate the various factors which determine the PT rate. Replacing His64 by alanine decreased the rates 20-fold, but they were restored when proton donors like imidazole and pyridine were added to the solution. In another series of mutants, the variation of the PT rate as a function of $\Delta pK_a = pK_a(\text{ZnH}_2\text{O}) - pK_a(\text{His64})$ could be studied. Similar studies were carried out on an isoenzyme, CAIII, where residue 64 is a lysine and proton transfers are two orders of magnitude slower. The crystal structure of CAII revealed that Zn and His64 are 7 \AA apart and that they are connected by a network of hydrogen-bonded water molecules. Moreover, the orientation of His64 with respect to the active site can easily change from inward to outward, fig. 2D. This rich set of data has motivated a number of theoretical studies. To specify the role of His64, the PMF was first calculated with and without His64²³⁵. The calculated values of $pK_a(\text{ZnH}_2\text{O})$, $pK_a(\text{His64})$ and ΔG^\ddagger were in good agreement with the data only when His64 was present in the inward orientation. The effect of the His64 to Ala mutation and the rescue by imidazole were also studied. Warshel's group was able to reproduce the variation of the PT rate as a function of ΔpK_a in CAIII by using a simplified PT chain made of His64, a water molecule and ZnOH^- (ref. 236). These studies underscore the importance of thermodynamic factors like the pK_a s of His64, of water molecules and more importantly of ZnH_2O , which must be close to 7 to ensure catalysis in both directions.

5 Conclusion

In this review we have shown how experimental and computational information can be combined to obtain mechanistic insight into enzyme catalysis that would not be possible to achieve by experimental or computational work alone. We have illustrated this point by discussing a few selected examples, focussing on enzymes that are relevant in the context of renewable fuel production: hydrogenases and carbon-monoxide dehydrogenase.

For reasons that we have discussed in the introduction, the catalytic mechanisms of enzymes that use inorganic active sites, such as those discussed in this review, is often

very difficult to study. Theoretical methods have been invaluable for predicting and understanding the molecular structure of intermediates by calculating their spectroscopic signatures, but the interplay between experiments and theory should also be useful for learning about the reactivity of these intermediates, and, about the kinetics of their chemical transformations. In particular, with regard to enzyme kinetics, the synergy arises because experimental methods typically report phenomenological rate constants characterising the overall process, whereas computational methods can help disentangle them to a set of rate constants of well defined elementary reaction steps. The ability to devise well defined model system, with infinite spatial resolution, is probably the greatest advantage of computational methods. Finding ways to connect computations on molecular models to actual experimental observations is arguably the greatest challenge.

Regarding the relative contributions of experimentalists and theoreticians in the elucidation of enzyme mechanisms, the question of which of the two plays the most important role is flawed, because the question assumes a two-step strategy where an initial proposal is simply followed by confirmation or refutation. In this review, we have attempted to describe another strategy where experimentalist and theoreticians work hand in hand and combine their expertise to obtain an answer more quickly and, hopefully, spread it over fewer papers.

6 Acknowledgment

This paper was partly written during a two-week residency in Marseille funded by the Mediterranean Institute for Advanced Research (www.imera.fr). P.-H.W. acknowledges the Ministry of Education, Republic of China (Taiwan), for a Ph.D. scholarship. J. B. acknowledges the Royal Society for a University Research Fellowship and the Engineering and Physical Sciences Research Council (EPSRC research grant EP/J015571/1) for financial support. L. D. G. acknowledges support from Ministero dell'Istruzione, dell'Università e della Ricerca (Prin 2010M2JARJ). The Marseille team acknowledges CNRS, Aix Marseille University, Région PACA, ANR (ANR12BS080014) for funding, and support from FrenchBIC (www.frenchbic.cnrs.fr).

References

- 1 C. Léger and P. Bertrand, *Chem. Rev.*, 2008, **108**, 2379–2438.
- 2 O. Rudiger, J. M. Abad, E. C. Hatchikian, V. M. Fernandez and A. L. de Lacey, *J. Am. Chem. Soc.*, 2005, **127**, 16008–16009.
- 3 C. Baffert, K. Sybirna, P. Ezanno, T. Lautier, V. Hajj, I. Meynial-Salles, P. Soucaille, H. Bottin and C. Léger, *Anal. Chem.*, 2012, **84**, 7999–8005.
- 4 C. Léger, F. Lederer, B. Guigliarelli and P. Bertrand, *J. Am. Chem. Soc.*, 2006, **128**, 180–187.
- 5 V. Fourmond, C. Baffert, K. Sybirna, T. Lautier, A. Abou Hamdan,

- 2306 S. Dementin, P. Soucaille, I. Meynial-Salles, H. Bottin and C. Léger, *J. Am. Chem. Soc.*, 2013, **135**, 3926–3938. 2368
- 2307 6 A. A. Hamdan, P.-P. Liebgott, V. Fourmond, O. Gutiérrez-Sanz, A. L. De Lacey, P. Infossi, M. Rousset, S. Dementin and C. Léger, *Proc. Nat. Acad. Sc. USA*, 2012, **109**, 19916–19921. 2369
- 2308 7 V. Hajj, C. Baffert, K. Sybirna, I. Meynial-Salles, P. Soucaille, H. Bottin, V. Fourmond and C. Léger, *Energy Environ. Sci.*, 2014, **7**, 715–719. 2370
- 2309 8 V. Fourmond, C. Greco, K. Sybirna, C. Baffert, P.-H. H. Wang, P. Ezanno, M. Montefiori, M. Bruschi, I. Meynial-Salles, P. Soucaille, J. Blumberger, H. Bottin, L. De Gioia and C. Léger, *Nature chemistry*, 2014, **6**, 336–342. 2371
- 2310 9 C. Léger, S. Dementin, P. Bertrand, M. Rousset and B. Guigliarelli, *J. Am. Chem. Soc.*, 2004, **126**, 12162–12172. 2372
- 2311 10 P.-P. Liebgott, F. Leroux, B. Burlat, S. Dementin, C. Baffert, T. Lautier, V. Fourmond, P. Ceccaldi, C. Cavazza, I. Meynial-Salles, P. Soucaille, J. C. C. Fontecilla-Camps, B. Guigliarelli, P. Bertrand, M. Rousset and C. Léger, *Nat. Chem. Biol.*, 2010, **6**, 63–70. 2373
- 2312 11 J. C. Fontecilla-Camps, A. Volbeda, C. Cavazza and Y. Nicolet, *Chem. Rev.*, 2007, **107**, 4273–4303. 2374
- 2313 12 W. Lubitz, H. Ogata, O. Rüdiger and E. Reijerse, *Chem. Rev.*, 2014, **114**, 4081–4148. 2375
- 2314 13 Y. Montet, P. Amara, A. Volbeda, X. Vernede, E. C. Hatchikian, M. J. Field, M. Frey and J. C. Fontecilla-Camps, *Nat. Struct. Mol. Biol.*, 1997, **4**, 523–526. 2376
- 2315 14 M. Bruschi, M. Tiberti, A. Guerra and L. De Gioia, *Journal of the American Chemical Society*, 2014, **136**, 1803–1814. 2377
- 2316 15 A. Silakov, B. Wenk, E. Reijerse and W. Lubitz, *Phys. Chem. Chem. Phys.*, 2009, **11**, 6592–6599. 2378
- 2317 16 G. Berggren, A. Adamska, C. Lambertz, T. R. Simmons, J. Esselborn, M. Atta, S. Gambarelli, J.-M. M. Mouesca, E. Reijerse, W. Lubitz, T. Happe, V. Artero and M. Fontecave, *Nature*, 2013, **499**, 66–69. 2379
- 2318 17 M. Can, F. A. Armstrong and S. W. Ragsdale, *Chemical reviews*, 2014, **114**, 4149–4174. 2380
- 2319 18 H. Drake, *Acetogenesis*, 1994, **3**. 2381
- 2320 19 P. Amara, J.-M. Mouesca, A. Volbeda and J. C. Fontecilla-Camps, *Inorg. Chem.*, 2011, **50**, 1868. 2382
- 2321 20 A. Warshel, J. K. Hwang and J. Aqvist, *Faraday Discuss.*, 1992, **93**, 225–238. 2383
- 2322 21 D. N. Silverman and S. Lindskog, *Acc. Chem. Res.*, 1988, **21**, 30–36. 2384
- 2323 22 P. E. M. Siegbahn and F. Himo, *J. Biol. Inorg. Chem.*, 2009, **14**, 643–651. 2385
- 2324 23 S. F. Sousa, P. A. Fernandes and M. J. Ramos, *Phys. Chem. Chem. Phys.*, 2012, **14**, 12431–12441. 2386
- 2325 24 T. A. A. Rokob, M. Srnc and L. Rulišek, *Dalton transactions (Cambridge, England : 2003)*, 2012, **41**, 5754–5768. 2387
- 2326 25 A. V. Nemukhin, B. L. Grigorenko, S. V. Lushchekina and S. D. Varfolomeev, *Russian Chemical Reviews*, 2012, **81**, 1011–1025. 2388
- 2327 26 P. E. Siegbahn and F. Himo, *Wiley Interdisciplinary Reviews: Computational Molecular Science*, 2011, **1**, 323–336. 2389
- 2328 27 M. Leopoldini, T. Marino, M. d. C. Michelini, I. Rivalta, N. Russo, E. Sicilia and M. Toscano, *Theoretical Chemistry Accounts*, 2007, **117**, 765–779. 2390
- 2329 28 T. Marino, N. Russo and M. Toscano, *J. Am. Chem. Soc.*, 2005, **127**, 4242–4253. 2391
- 2330 29 O. Amata, T. Marino, N. Russo and M. Toscano, *J. Am. Chem. Soc.*, 2011, **133**, 17824–17831. 2392
- 2331 30 M. E. Alberto, T. Marino, N. Russo, E. Sicilia and M. Toscano, *Phys. Chem. Chem. Phys.*, 2012, **14**, 14943–14953. 2393
- 2332 31 A. Klamt, *J. Phys. Chem.*, 1995, **99**, 2224–2235. 2394
- 2333 32 A. Klamt, *J. Phys. Chem.*, 1996, **100**, 3349–3353. 2395
- 2334 33 A. Klamt and G. Schuurmann, *J. Chem. Soc., Perkin Trans. 2*, 1993, **0**, 799–805. 2396
- 34 J. Andzelm, C. Kolmel and A. Klamt, *The Journal of Chemical Physics*, 1995, **103**, 9312. 2397
- 35 J. Tomasi, B. Mennucci and R. Cammi, *Chem. Rev.*, 2005, **105**, 2999–3094. 2398
- 36 M. Cossi, N. Rega, G. Scalmani and V. Barone, *J. Comput. Chem.*, 2003, **24**, 669–681. 2399
- 37 M. Cossi, G. Scalmani, N. Rega and V. Barone, *The Journal of Chemical Physics*, 2002, **117**, 43–54. 2400
- 38 V. Barone and M. Cossi, *J. Phys. Chem. A*, 1998, **102**, 1995–2001. 2401
- 39 J. Tomasi and M. Persico, *Chem. Rev.*, 1994, **94**, 2027–2094. 2402
- 40 N. Rega, M. Cossi, V. Barone, C. Pomelli and J. Tomasi, *Int. J. Quantum Chem.*, 1999, **73**, 219–227. 2403
- 41 A. Warshel and M. Levitt, *Journal of Molecular Biology*, 1976, **103**, 227–249. 2404
- 42 U. Ryde, *Dalton Trans.*, 2007, 607–625. 2405
- 43 U. Ryde, C. Greco and L. De Gioia, *Journal of the American Chemical Society*, 2010, **132**, 4512–4513. 2406
- 44 A. Silakov, C. Kamp, E. Reijerse, T. Happe and W. Lubitz, *Biochemistry*, 2009, **48**, 7780–7786. 2407
- 45 A. Volbeda, M. H. Charon, C. Piras, E. C. Hatchikian, M. Frey and J. C. Fontecilla-Camps, *Nature*, 1995, **373**, 580–587. 2408
- 46 H.-J. Fan and M. B. Hall, *J. Am. Chem. Soc.*, 2001, **123**, 3828–3829. 2409
- 47 J. G. Norman, P. B. Ryan and L. Noodleman, *J. Am. Chem. Soc.*, 1980, **102**, 4279–4282. 2410
- 48 L. Noodleman, *The Journal of Chemical Physics*, 1981, **74**, 5737–5743. 2411
- 49 L. Yu, C. Greco, M. Bruschi, U. Ryde, L. De Gioia and M. Reiher, *Inorg. Chem.*, 2011, **50**, 3888–3900. 2412
- 50 J. W. Tye, M. Y. Darensbourg and M. B. Hall, *J. Comput. Chem.*, 2006, **27**, 1454–1462. 2413
- 51 J. W. Tye, M. Y. Darensbourg and M. B. Hall, *Inorg. Chem.*, 2008, **47**, 2380–2388. 2414
- 52 T. Ziegler and J. Autschbach, *Chemical reviews*, 2005, **105**, 2695–2722. 2415
- 53 S. P. de Visser, M. G. Quesne, B. Martin, P. Comba and U. Ryde, *Chem. Commun.*, 2014, **50**, 262–282. 2416
- 54 C. J. Cramer and D. G. Truhlar, *Phys. Chem. Chem. Phys.*, 2009, **11**, 10757–10816. 2417
- 55 F. Neese, *J. Biol. Inorg. Chem.*, 2006, **11**, 702–711. 2418
- 56 J. L. Chen, L. Noodleman, D. A. Case and D. Bashford, *J. Phys. Chem.*, 1994, **98**, 11059–11068. 2419
- 57 W. Pritzkow, *J. Prakt. Chem.*, 1998, **340**, 586–587. 2420
- 58 J. Bigeleisen and M. G. Mayer, *The Journal of Chemical Physics*, 1947, **15**, 261. 2421
- 59 A. Cornish-Bowden, *Fundamental of Enzyme kinetics*, Portland Press., 2004. 2422
- 60 M. G. Almeida, B. Guigliarelli, P. Bertrand, J. J. G. Moura, I. Moura and C. Léger, *FEBS Letts.*, 2007, **581**, 284–288. 2423
- 61 V. Fourmond, C. Baffert, K. Sybirna, S. Dementin, A. Abou-Hamdan, I. Meynial-Salles, P. Soucaille, H. Bottin and C. Léger, *Chem. Commun.*, 2013, **49**, 6840–6842. 2424
- 62 M. Y. Okamura, R. A. Isaacson and G. Feher, *Biochimica et Biophysica Acta (BBA) - Bioenergetics*, 1979, **546**, 394–417. 2425
- 63 A. Abou Hamdan, S. Dementin, P.-P. Liebgott, O. Gutierrez-Sanz, P. Richaud, A. L. De Lacey, M. Rousset, P. Bertrand, L. Cournac and C. Léger, *J. Am. Chem. Soc.*, 2012, **134**, 8368–8371. 2426
- 64 R. O. Louro, T. Catarino, C. M. Paquete and D. L. Turnera, *FEBS Lett.*, 2004, **576**, 77–80. 2427
- 65 M. Tegoni, M. C. Silvestrini, B. Guigliarelli, M. Asso, M. Brunori and P. Bertrand, *Biochemistry*, 1998, **37**, 12761–12771. 2428
- 66 D. L. Williams-Smith, R. C. Bray, M. J. Barber, A. D. Tsopanakakis and S. P. Vincent, *The Biochemical journal*, 1977, **167**, 593–600. 2429
- 67 V. Fourmond, B. Burlat, S. Dementin, P. Arnoux, M. Sabaty, S. Boiry, B. Guigliarelli, P. Bertrand, D. Pignol and C. Léger, *J. Phys. Chem. B*, 2430

- 2008, **112**, 15478–15486.
- 2430 68 J. M. Savéant, *Elements of molecular and biomolecular electrochem-* 2492
2431 *istry*, John Wiley & sons, Inc., 2006. 2493
- 2432 69 K. Chen, J. Hirst, R. Camba, C. A. Bonagura, C. D. Stout, B. K. Burgess 2494
2433 and F. A. Armstrong, *Nature*, 2000, **405**, 814–817. 2495
- 2434 70 A. K. Jones, R. Camba, G. A. Reid, S. K. Chapman and F. A. Armstrong, 2496
2435 *J. Am. Chem. Soc.*, 2000, **122**, 6494–6495. 2497
- 2436 71 C. Léger, A. K. Jones, W. Roseboom, S. P. J. Albracht and F. A. Arm- 2498
2437 strong, *Biochemistry*, 2002, **41**, 15736–15746. 2499
- 2438 72 P. Bertrand, B. Frangioni, S. Dementin, M. Sabaty, P. Arnoux, 2500
2439 B. Guigliarelli, D. Pignol and C. Léger, *J. Phys. Chem. B*, 2007, **111**, 2502
2440 10300–10311.
- 2441 73 C. Léger, A. K. Jones, S. P. J. Albracht and F. A. Armstrong., *J. Phys.* 2503
2442 *Chem. B*, 2002, **106**, 13058–13063. 2504
- 2443 74 D. Yepes, R. Seidel, B. Winter, J. Blumberger and P. Jaque, *J. Phys.* 2505
2444 *Chem. B*, 2014, 6850–6863. 2506
- 2445 75 A. Warshel, *J. Phys. Chem.*, 1982, **86**, 2218. 2507
- 2446 76 J. Blumberger and M. L. Klein, *J. Am. Chem. Soc.*, 2006, **128**, 13854. 2508
- 2447 77 J. Blumberger, *Phys. Chem. Chem. Phys*, 2008, **10**, 5651. 2509
- 2448 78 J. Moens, R. Seidel, P. Geerlings, M. Faubel, B. Winter and J. Blum- 2510
2449 berger, *J. Phys. Chem. B*, 2010, **114**, 9173–9182. 2511
- 2450 79 Y. Tateyama, J. Blumberger, T. Ohno and M. Sprik, *The Journal of* 2512
2451 *Chemical Physics*, 2007, **126**, 204506+. 2513
- 2452 80 H. Oberhofer and J. Blumberger, *Angew. Chem. Int. Ed.*, 2010, **49**, 3631. 2514
- 2453 81 M. H. M. Olsson, G. Hong and A. Warshel, *J. Am. Chem. Soc.*, 2003, 2515
2454 **125**, 5025. 2516
- 2455 82 M. Breuer, P. Zarzycki, J. Blumberger and K. M. Rosso, *J. Am. Chem.* 2517
2456 *Soc.*, 2012, **134**, 9868–9871. 2518
- 2457 83 A. P. Gamiz-Hernandez, G. Kieseritzki, H. Ishikita and E. W. Knapp, *J.* 2519
2458 *Chem. Theory. Comput.*, 2011, **7**, 742. 2520
- 2459 84 Marian Breuer, Kevin M. Rosso, Jochen Blumberger and Julea N. Butt 2521
2460 "Multi-heme Cytochromes : Structures, functions and opportunities", *J.* 2522
2461 *R. Soc. Interface* (2014), under review. 2523
- 2462 85 B. M. Fonseca, C. M. Paquete, C. A. Salgueiro and R. O. Louro, *FEBS* 2524
2463 *letters*, 2012, **586**, 504–509. 2525
- 2464 86 M. Pessanha, E. L. Rothery, C. S. Miles, G. A. Reid, S. K. Chapman, 2526
2465 R. O. Louro, D. L. Turner, C. A. Salgueiro and A. V. Xavier, *Biochimica* 2527
2466 *et Biophysica Acta (BBA) - Bioenergetics*, 2009, **1787**, 113–120. 2528
- 2467 87 J. Alric, J. Lavergne, F. Rappaport, A. Vermeglio, K. Matsuura, K. Shi- 2529
2468 mada and K. V. P. Nagashima, *J. Am. Chem. Soc.*, 2006, **128**, 4136–4145. 2530
- 2469 88 M. R. Gunner, M. A. Saleh, E. Cross, A. ud Doula and M. Wise, *Bio-* 2531
2470 *physical Journal*, 2000, **78**, 1126. 2532
- 2471 89 D. S. Spencer, D. Weiss, W. E. Stites, B. Garcia-Moreno, J. J. Dwyer, 2533
2472 A. G. Gittis and E. E. Lattman, *Biophysical Journal*, 1998, **74**, A170. 2534
- 2473 90 J. J. Dwyer, A. G. Gittis, D. A. Karp, E. E. Lattman, D. S. Spencer, W. E. 2535
2474 Stites and B. Garcia-Moreno, *Biophysical Journal*, 2000, **79**, 1610– 2536
2475 1620. 2537
- 2476 91 C. A. Fitch, D. A. Karp, K. K. Lee, W. E. Stites, E. E. Lattman and 2538
2477 B. Garcia-Moreno, *Biophysical Journal*, 2002, **82**, 3289–3304. 2539
- 2478 92 Y. Takayama, C. A. Castaneda, M. Chimentin, B. Garcia-Moreno and 2540
2479 J. Iwahara, *Journal of the American Chemical Society*, 2008, **130**, 6714– 2541
2480 6715. 2542
- 2481 93 A. L. Hansen and L. E. Key, *Proceedings of the National Academy of* 2543
2482 *Sciences of the USA*, 2014, **ASAP**, E1705–E1712. 2544
- 2483 94 S. Farrjones, W. Wong, W. Guthel and W. Bachovchin, *Journal of the* 2545
2484 *American Chemical Society*, 1993, **115**, 6813–6819. 2546
- 2485 95 P. Kucik, D. Farrell, L. P. McIntosh, B. Garcia-Moreno, K. S. Jensen, 2547
2486 Z. Toleikis, K. Teilum and J. J. Nielsen, *Journal of the American Chemi-* 2548
2487 *cal Society*, 2013, **135**, 16978–16976. 2549
- 2488 96 E. Alexov, E. L. Mehler, N. Baker, A. M. Baptista, Y. Huang, F. Milletti, 2550
2489 J. E. Nielsen, D. Farrell, T. Carstensen, M. H. M. Olsson, J. K. Shen, 2551
2490 J. Warwicker, S. Williams and J. M. Word, *Proteins-Structure Function* 2552
2491 *and Bioinformatics*, 2011, **79**, 3260–3275. 2553
- 97 C. Tanford and J. G. Kirkwood, *J. Am. Chem. Soc.*, 1957, **79**, 5333– 2493
5339. 2494
- 98 Y. F. Song, J. J. Mao and M. R. Gunner, *Biochemistry*, 2003, **42**, 9875– 2495
9888. 2496
- 99 M. J. Ondrechen, J. G. Clifton and D. Ringe, *Proceedings of the National* 2497
2498 *Academy of Sciences of the USA*, 2001, **98**, 12473–12478. 2499
- 100 H. Ishikita, G. Morra and E. W. Knapp, *Biochemistry*, 2003, **42**, 3882– 2500
3892. 2501
- 101 T. Simonson and D. Perahia, *Proceedings of the National Academy of* 2502
2503 *Sciences of the USA*, 1995, **92**, 1082–1086. 2504
- 102 M. R. Gunner and E. Alexov, *Biochimica Et Biophysica Acta-* 2505
2506 *Bioenergetics*, 2000, **1458**, 63–87. 2507
- 103 C. N. Schutz and A. Warshel, *Proteins-Structure Function and Genetics*, 2508
2509 2001, **44**, 400–417. 2510
- 104 J. Ho and M. L. Coote, *Wiley Interdisciplinary Reviews-Computational* 2511
2512 *Molecular Science*, 2011, **1**, 649–660. 2513
- 105 J. Ho and M. L. Coote, *Theoretical Chemistry Accounts*, 2010, **125**, 3– 2514
21. 2515
- 106 J. Ho, C. J. Easton and M. L. Coote, *Journal of the American Chemical* 2516
2517 *Society*, 2010, **132**, 5515–5521. 2518
- 107 A. M. Rebolgar-Zepeda and A. Galano, *International Journal of Quantum* 2519
2520 *Chemistry*, 2012, **112**, 3449–3460. 2521
- 108 M. Mangold, L. Rolland, F. Costanzo, M. Sprik, M. Sulpizi and J. Blum- 2522
2523 berger, *J. Chem. Theory Comput.*, 2011, **7**, 1951–1961. 2524
- 109 J. R. Pliengo and J. M. Riveros, *Journal of Physical Chemistry A*, 2001, 2525
2526 **105**, 7241–7247. 2527
- 110 A. M. Rebolgar-Zepeda, T. Campos-Hernandez, M. T. Ramirez-Silva, 2528
2529 A. Rojas-Hernandez and A. Galano, *Journal of Chemical Theory and* 2529
2530 *Computation*, 2011, **7**, 2528–2538. 2531
- 111 H. Li, A. D. Robertson and J. H. Jensen, *Proteins-Structure Function* 2532
2533 *and Bioinformatics*, 2004, **55**, 689–704. 2534
- 112 J. H. Jensen, H. Li, A. D. Robertson and P. A. Molina, *Journal of Physical* 2535
2536 *Chemistry A*, 2005, **109**, 6634–6643. 2537
- 113 Z. Y. Zhu and M. R. Gunner, *Biochemistry*, 2005, **44**, 82–96. 2538
- 114 R. E. Georgescu, E. G. Alexov and M. R. Gunner, *Biophysical Journal*, 2539
2540 2002, **83**, 1731–1748. 2541
- 115 J. Antosiewicz, J. A. McCammon and M. K. Gilson, *Biochemistry*, 1996, 2542
2543 **35**, 7819–7833. 2544
- 116 L. Sandberg and O. Edholm, *Proteins-Structure Function and Genetics*, 2545
2546 1999, **36**, 474–483. 2547
- 117 I. Muegge, P. X. Qi, A. J. Wand, Z. T. Chu and A. Warshel, *Journal of* 2548
2549 *Physical Chemistry A*, 1997, **101**, 825–836. 2550
- 118 T. Simonson, J. Carlsson and D. A. Case, *Journal of the American Chemi-* 2551
2552 *cal Society*, 2004, **126**, 4167–4180. 2553
- 119 Y. Song, J. Mao and M. R. Gunner, *Journal of Computational Chemistry*, 2554
2555 2009, **30**, 2231–2247. 2556
- 120 Y. Y. Sham, Z. T. Chu, H. H. Tao and A. Warshel, *Proteins-Structure* 2557
2558 *Function and Genetics*, 2000, **39**, 393–407. 2559
- 121 J. A. Wallace and J. K. Shen, *Journal of Chemical Theory and Compu-* 2560
2561 *tation*, 2011, **7**, 2617–2629. 2562
- 122 S. L. Williams, C. A. F. de Oliveira and A. J. McCammon, *Journal of* 2563
2564 *Chemical Theory and Computation*, 2010, **6**, 560–568. 2565
- 123 A. M. Baptista, P. J. Martel and S. B. Petersen, *Proteins-Structure Func-* 2566
2567 *tion and Genetics*, 1997, **27**, 523–544. 2568
- 124 A. M. Baptista, V. H. Teixeira and C. M. Soares, *Journal of Chemical* 2569
2570 *Physics*, 2002, **117**, 4184–4200. 2571
- 125 W. J. Ray, *Biochemistry*, 1983, **22**, 4625–4637. 2572
- 126 K. J. Laidler, *J. Chem. Educ.*, 1988, **65**, 250+. 2573
- 127 S. Dementin, B. Burlat, V. Fourmond, F. Leroux, P.-P. P. Liebgott, 2574
2575 A. Abou Hamdan, C. Léger, M. Rousset, B. Guigliarelli and P. Bertrand, 2576
2577 *J. Am. Chem. Soc.*, 2011, **133**, 10211–10221. 2578

- 2554 128 J. Gao, in *Reaction Rate Constant Computations : Theories and Appli-*
2555 *cations*, ed. T. C. Keli Han, RSC, 2013, ch. Molecular Dynamics Simu-
2556 lation of Kinetic Isotope Effects in Enzyme-Catalyzed Reactions.
- 2557 129 J. Blumberger and M. L. Klein, *Chem. Phys. Lett.*, 2006, **422**, 210.
- 2558 130 P. Bertrand, in *Reaction Rate Constant Computations : Theories and*
2559 *Applications*, ed. T. C. Keli Han, RSC, 2013, ch. Molecular Modelling
2560 of Proton Transfer Kinetics in Biological Systems.
- 2561 131 R. Elber, *Current Opinion in Structural Biology*, 2010, **20**, 162–167.
- 2562 132 T. Lautier, P. Ezanno, C. Baffert, V. Fourmond, L. Cournac, J. C.
2563 Fontecilla-Camps, P. Soucaille, P. Bertrand, I. Meynial-Salles and
2564 C. Léger, *Faraday discussions*, 2011, **148**, 385–407.
- 2565 133 S. Riistama, A. Puustinen, M. I. Verkhovsky, J. E. Morgan and M. Wik-
2566 strom, *Biochemistry*, 2000, **39**, 6365–6372.
- 2567 134 L. Salomonsson, A. Lee, R. B. Gennis and P. Brzezinski, *Proc. Nat.*
2568 *Acad. Sci. USA*, 2004, **101**, 11617–11621.
- 2569 135 F. Leroux, S. Dementin, B. Burlat, L. Cournac, A. Volbeda, S. Champ,
2570 L. Martin, B. Guigliarelli, P. Bertrand, J. Fontecilla-Camps, M. Rousset
2571 and C. Léger, *Proc. Nat. Acad. Sci. USA*, 2008, **105**, 11188–11193.
- 2572 136 G. Goldet, C. Brandmayr, S. T. Stripp, T. Happe, C. Cavazza, J. C.
2573 Fontecilla-Camps and F. A. Armstrong, *J. Am. Chem. Soc.*, 2009, **131**,
2574 14979–14989.
- 2575 137 V. H. Teixeira, A. M. Baptista and C. M. Soares, *Biophys. J.*, 2006, **91**,
2576 2035.
- 2577 138 J. Z. Ruscio, D. Kumar, M. Shukla, M. G. Prisant, T. M. Murali and
2578 A. V. Onufriev, *Proc. Natl. Acad. Sci. USA*, 2008, **105**, 9204.
- 2579 139 R. Baron, C. Riley, P. Chenprakhon, K. Thotsaporn, R. T. Winter, A. Al-
2580 fieri, F. Forneris, W. J. H. van Berkel, P. Chaiyen, M. W. Fraaije, A. Mat-
2581 tevi and J. A. McCammon, *Proc. Natl. Acad. Sci. USA*, 2009, **106**,
2582 10603.
- 2583 140 M. D'Abramo, A. Di Nola and A. Amadei, *J. Phys. Chem. B*, 2009, **113**,
2584 16346.
- 2585 141 R. Elber and M. Karplus, *J. Am. Chem. Soc.*, 1990, **112**, 9161.
- 2586 142 J. Cohen, K. Kim, M. Posewitz, M. L. Ghirardi, K. Schulten, M. Seibert
2587 and P. King, *Biochemical Society Transactions*, 2005, **33**, 80.
- 2588 143 J. Cohen, K. Kim, P. King, M. Seibert and K. Schulten, *Structure*, 2005,
2589 **13**, 1321.
- 2590 144 J. Cohen, A. Arkhipov, R. Braun and K. Schulten, *Biophys. J.*, 2006, **91**,
2591 1844.
- 2592 145 J. Cohen and K. Schulten, *Biophys. J.*, 2007, **93**, 3591.
- 2593 146 Y. Nishihara, S. Hayashi and S. Kato, *Chem. Phys. Lett.*, 2008, **464**, 220.
- 2594 147 M. Ceccarelli, R. Anedda, M. Casu and P. Ruggerone, *Proteins*, 2008,
2595 **71**, 1231.
- 2596 148 L. Maragliano, G. Cottone, G. Ciccotti and E. Vanden-Eijnden, *J. Am.*
2597 *Chem. Soc.*, 2009, **132**, 1010.
- 2598 149 P.-L. Liebgott, F. Leroux, B. Burlat, S. Dementin, C. Baffert, T. Lau-
2599 tier, V. Fourmond, P. Ceccaldi, C. Cavazza, I. Meynial-Salles, P. Sou-
2600 caille, J. C. Fontecilla-Camps, B. Guigliarelli, P. Bertrand, M. Rousset
2601 and C. Léger, *Nat. Chem. Biol.*, 2010, **6**, 63.
- 2602 150 P. Wang, R. B. Best and J. Blumberger, *J. Am. Chem. Soc.*, 2011, **133**,
2603 3548.
- 2604 151 P. Wang, R. B. Best and J. Blumberger, *Phys. Chem. Chem. Phys.*, 2011,
2605 **13**, 7708.
- 2606 152 P. Wang and J. Blumberger, *Proc. Natl. Acad. Sci. USA*, 2012, **109**, 6399.
- 2607 153 P. Wang, M. Bruschi, L. De Gioia and J. Blumberger, *J. Am. Chem. Soc.*,
2608 2013, **135**, 9493.
- 2609 154 Y. Shomura, K.-S. Yoon, H. Nishihara and Y. Higuchi, *Nature*, 2011,
2610 **479**, 253–256.
- 2611 155 J. Fritsch, P. Scheerer, S. Frielingsdorf, S. Kroschinsky, B. Friedrich,
2612 O. Lenz and C. M. Spahn, *Nature*, 2011, **479**, 249–252.
- 2613 156 M.-E. E. Pandelia, D. Bykov, R. Izsak, P. Infossi, M.-T. T. Giudici-
2614 Orticoni, E. Bill, F. Neese and W. Lubitz, *Proceedings of the National*
2615 *Academy of Sciences of the United States of America*, 2013, **110**, 483–
488.
- 2616 157 R. Cammack, D. Patil, R. Aguirre and E. Hatchikian, *FEBS Letters*,
2617 1982, **142**, 289–292.
- 2618 158 V. M. Fernandez, E. C. Hatchikian, D. S. Patil and R. Cammack,
2619 *Biochim. Biophys. Acta*, 1986, **883**, 145–154.
- 2620 159 S. L. Lamle, S. P. J. Albracht and F. A. Armstrong, *J. Am. Chem. Soc.*,
2621 2004, **126**, 14899–14909.
- 2622 160 J. A. Cracknell, A. F. Wait, O. Lenz, B. Friedrich and F. A. Armstrong,
2623 *Proc. Nat. Acad. Sci. USA*, 2009, **106**, 20681–20686.
- 2624 161 M.-E. Pandelia, V. Fourmond, P. Tron-Infossi, E. Lojou, P. Bertrand,
2625 C. Léger, M.-T. Giudici-Orticoni and W. Lubitz, *J. Am. Chem. Soc.*,
2626 2010, **132**, 6991–7004.
- 2627 162 V. Fourmond, P. Infossi, M.-T. Giudici-Orticoni, P. Bertrand and
2628 C. Léger, *J. Am. Chem. Soc.*, 2010, **132**, 4848–4857.
- 2629 163 M.-E. Pandelia, W. Nitschke, P. Infossi, M.-T. Giudici-Orticoni, E. Bill
2630 and W. Lubitz, *Proc. Natl. Acad. Sci. U.S.A.*, 2011, **108**, 6097–6102.
- 2631 164 M. J. Lukey, M. M. Roessler, A. Parkin, R. M. Evans, R. A. Davies,
2632 O. Lenz, B. Friedrich, F. Sargent and F. A. Armstrong, *J. Am. Chem.*
2633 *Soc.*, 2011, **133**, 16881–16892.
- 2634 165 S. Frielingsdorf, J. Fritsch, A. Schmidt, M. Hammer, J. Lwenstein,
2635 E. Siebert, V. Pelmenshikov, T. Jaenicke, J. Kalms, Y. Rippers,
2636 F. Lendzian, I. Zebger, C. Teutloff, M. Kaupp, R. Bittl, P. Hildebrandt,
2637 B. Friedrich, O. Lenz and P. Scheerer, *Nat. Chem. Biol.*, 2014, **10**, 378–
2638 385.
- 2639 166 A. Volbeda, P. Amara, C. Darnault, J.-M. Mouesca, A. Parkin, M. M.
2640 Roessler, F. A. Armstrong and J. C. Fontecilla-Camps, *Proc. Natl. Acad.*
2641 *Sci. U.S.A.*, 2012, **109**, 5305–5310.
- 2642 167 R. M. Evans, A. Parkin, M. M. Roessler, B. J. Murphy, H. Adamson,
2643 M. J. Lukey, F. Sargent, A. Volbeda, J. C. Fontecilla-Camps and F. A.
2644 Armstrong, *J. Am. Chem. Soc.*, 2013, **135**, 2694–2707.
- 2645 168 A. Volbeda, Y. Montet, X. Vernède, E. Hatchikian and J. C. Fontecilla-
2646 Camps, *International Journal of Hydrogen Energy*, 2002, **27**, 1449–
2647 1461.
- 2648 169 T. Buhre, O. Lenz, N. Krauss and B. Friedrich, *J. Biol. Chem.*, 2005,
2649 **280**, 23791–23796.
- 2650 170 O. Duché, S. Elsen, L. Cournac and A. Colbeau, *FEBS J.*, 2005, **272**,
2651 3899–3908.
- 2652 171 V. H. Teixeira, A. M. Baptista and C. M. Soares, *Biophys. J.*, 2006, **91**,
2653 2035–2045.
- 2654 172 B. Jähne, G. Heinz and W. Dietrich, *J. Geophys. Res.*, 1987, **92**, 10767.
- 2655 173 A. Akgerman and J. Gainer, *Ind. Eng. Chem. Fund.*, 1972, **11**, 373.
- 2656 174 A. Akgerman and J. Gainer, *J. Chem. Eng. Data*, 1972, **17**, 372.
- 2657 175 D. R. Lide, *CRC Handbook of Chemistry and Physics*, CRC Press, 1995.
- 2658 176 B. Kowert and N. Dang, *J. Phys. Chem. A*, 1999, **103**, 779.
- 2659 177 M. J. W. Frank, J. A. M. Kuipers and W. P. M. van Swaaij, *J. Chem. Eng.*
2660 *Data*, 1996, **41**, 297.
- 2661 178 E. L. Maynard and P. A. Lindahl, *J. Am. Chem. Soc.*, 1999, **121**, 9221.
- 2662 179 J. Seravalli and S. W. Ragsdale, *Biochemistry*, 2000, **39**, 1274.
- 2663 180 C. Darnault, A. Volbeda, E. J. Kim, P. Legrand, X. Vernède, P. A. Lin-
2664 dahl and J. C. Fontecilla-Camps, *Nature Struct. Molec. Biol.*, 2003, **10**,
2665 271.
- 2666 181 T. I. Doukov, T. M. Iverson, J. Seravalli, S. W. Ragsdale and C. L. Dren-
2667 nan, *Science*, 2002, **298**, 567.
- 2668 182 T. I. Doukov, L. C. Blasiak, J. Seravalli, S. W. Ragsdale and C. L. Dren-
2669 nan, *Biochemistry*, 2008, **47**, 3474.
- 2670 183 X. Tan, H. Loke, S. Fitch and P. Lindahl, *J. Am. Chem. Soc.*, 2005, **127**,
2671 5833.
- 2672 184 A. Volbeda and J. Fontecilla-Camps, *J. Biol. Inorg. Chem.*, 2004, **9**, 525.
- 2673 185 X. Tan, A. Volbeda, J. Fontecilla-Camps and P. Lindahl, *J. Biol. Inorg.*
2674 *Chem.*, 2006, **11**, 371.
- 2675 186 M. Kumar, W. P. Lu, L. Liu and S. W. Ragsdale, *J. Am. Chem. Soc.*,
2676 1993, **115**, 11646.
- 2677

- 2678 187 C. Baffert, L. Bertini, T. Lautier, C. Greco, K. Sybirna, P. Ezanno, E. Etienne, P. Soucaille, P. Bertrand, H. Bottin, I. Meynial-Salles, L. De Gioia and C. Léger, *J. Am. Chem. Soc.*, 2011, **133**, 2096–2099.
- 2679
- 2680
- 2681 188 C. E. Foster, T. Krmer, A. F. Wait, A. Parkin, D. P. Jennings, T. Happe, J. E. McGrady and F. A. Armstrong, *J. Am. Chem. Soc.*, 2012, **134**, 7553–7557.
- 2682
- 2683
- 2684 189 A. Adamska, A. Silakov, C. Lambertz, O. Rüdiger, T. Happe, E. Reijerse and W. Lubitz, *Angewandte Chemie (International ed. in English)*, 2012, **51**, 11458–11462.
- 2685
- 2686
- 2687 190 L. Bertini, C. Greco, M. Bruschi, P. Fantucci and L. De Gioia, *Organometallics*, 2010, **29**, 2013–2025.
- 2688
- 2689 191 J. Esselborn, C. Lambertz, A. Adamska-Venkatesh, T. Simmons, G. Berggren, J. Noth, J. Siebel, A. Hemschemeier, V. Artero, E. Reijerse, M. Fontecave, W. Lubitz and T. Happe, *Nat. Chem. Biol.*, 2013, **9**, 607–609.
- 2690
- 2691
- 2692
- 2693 192 D. W. Mulder, E. S. Boyd, R. Sarma, R. K. Lange, J. A. Endrizzi, J. B. Broderick and J. W. Peters, *Nature*, 2010, **465**, 248–251.
- 2694
- 2695 193 C. Baffert, M. Demuez, L. Cournac, B. Burlat, B. Guigliarelli, P. Soucaille, P. Bertrand, L. Girbal and C. Léger, *Angew. Chem. Int. Edit.*, 2008, **47**, 2052–2055.
- 2696
- 2697
- 2698 194 B. Bennett, B. J. Lemon and J. W. Peters, *Biochemistry*, 2000, **39**, 7455–7460.
- 2699
- 2700 195 S. T. Stripp, G. Goldet, C. Brandmayr, O. Sanganas, K. A. Vincent, M. Haumann, F. A. Armstrong and T. Happe, *Proc. Nat. Acad. Sc. USA*, 2009, **106**, 17331–17336.
- 2701
- 2702
- 2703 196 M. T. Stiebritz and M. Reiher, *Inorg. Chem.*, 2009, **48**, 7127–7140.
- 2704
- 2705 197 M. T. Stiebritz and M. Reiher, *Inorg. Chem.*, 2010, **49**, 8645.
- 2706
- 2707 198 G. Hong and R. Pachter, *ACS chemical biology*, 2012, **7**, 1268–1275.
- 2708
- 2709 199 A. Kubas, D. De Sancho, R. B. Best and J. Blumberger, *Angew. Chem. Int. Ed. Engl.*, 2014, **53**, 4081–4084.
- 2710
- 2711 200 C. Lambertz, N. Leidel, K. G. V. Havelius, J. Noth, P. Chernev, M. Winkler, T. Happe and M. Haumann, *J. Biol. Chem.*, 2011, **286**, 40614–40623.
- 2712
- 2713 201 M. K. Bruska, M. T. Stiebritz and M. Reiher, *J. Am. Chem. Soc.*, 2011, **133**, 20588–20603.
- 2714
- 2715 202 A. S. Pandey, T. V. Harris, L. J. Giles, J. W. Peters and R. K. Szilagy, *J. Am. Chem. Soc.*, 2008, **130**, 4533–4540.
- 2716
- 2717 203 A. Parkin, C. Cavazza, J. Fontecilla-Camps and F. Armstrong, *J. Am. Chem. Soc.*, 2006, **128**, 16808–16815.
- 2718
- 2719 204 M. T. Olsen, T. B. Rauchfuss and S. R. Wilson, *J. Am. Chem. Soc.*, 2010, **132**, 17733–17740.
- 2720
- 2721 205 T. Miyake, M. Bruschi, U. Cosentino, C. Baffert, V. Fourmond, C. Léger, G. Moro, L. Gioia and C. Greco, *J. Biol. Inorg. Chem.*, 2013, **18**, 693–700.
- 2722
- 2723 206 V. Fourmond, P. Infossi, M.-T. Giudici-Ortoni, P. Bertrand and C. Léger, *J. Am. Chem. Soc.*, 2010, **132**, 4848–4857.
- 2724
- 2725 207 J. G. J. Jacques, B. Burlat, P. Arnoux, M. Sabaty, B. Guigliarelli, C. Léger, D. Pignol and V. Fourmond, *Biochimica et Biophysica Acta (BBA) - Bioenergetics*, 2014, **1837**, 1801–1809.
- 2726
- 2727 208 J. W. Peters, W. N. Lanzilotta, B. J. Lemon and L. C. Seefeldt, *Science*, 1998, **282**, 1853–1858.
- 2728
- 2729 209 C. Greco, M. Bruschi, P. Fantucci, U. Ryde and L. DeGioia, *Chem. Eur. J.*, 2011, **17**, 1954–1965.
- 2730
- 2731 210 I. Fdez Galván, A. Volbeda, J. C. Fontecilla-Camps and M. J. Field, *Proteins*, 2008, **73**, 195–203.
- 2732
- 2733 211 V. H. Teixeira, C. M. Soares and A. M. Baptista, *Proteins*, 2008, **70**, 1010–1022.
- 2734
- 2735 212 P. M. Matias, C. M. Soares, L. M. Saraiva, R. Coelho, J. Morais, J. Le Gall and M. A. Carrondo, *Journal of biological inorganic chemistry : JBIC : a publication of the Society of Biological Inorganic Chemistry*, 2001, **6**, 63–81.
- 2736
- 2737
- 2738
- 2739 213 S. Dementin, V. Belle, P. Bertrand, B. Guigliarelli, G. Adryanczyk-Perrier, A. Delacey, V. M. Fernandez, M. Rousset and C. Léger, *J. Am. Chem. Soc.*, 2006, **128**, 5209–5218.
- 2740
- 2741 214 D. N. Beratan, J. N. Betts and J. N. Onuchic, *Science*, 1991, **252**, 1285–1288.
- 2742
- 2743 215 M.-L. L. Tan, I. Balabin and J. N. N. Onuchic, *Biophysical journal*, 2004, **86**, 1813–1819.
- 2744
- 2745 216 T. R. Prytkova, I. V. Kurnikov and D. N. Beratan, *The journal of physical chemistry. B*, 2005, **109**, 1618–1625.
- 2746
- 2747 217 A. A. Stuchebrukhov, *Theoretical Chemistry Accounts*, 2003, **110**, 291–306.
- 2748
- 2749 218 D. M. Smith, K. M. Rosso, M. Dupuis, M. Valiev and T. P. Straatsma, *The journal of physical chemistry. B*, 2006, **110**, 15582–15588.
- 2750
- 2751 219 M. Breuer, K. M. Rosso and J. Blumberger, *Proceedings of the National Academy of Sciences*, 2014, **111**, 611–616.
- 2752
- 2753 220 G. Hong, A. J. Cornish, E. L. Hegg and R. Pachter, *Biochimica et biophysica acta*, 2011, **1807**, 510–517.
- 2754
- 2755 221 B. Ginovska-Pangovska, M.-H. H. Ho, J. C. Linehan, Y. Cheng, M. Dupuis, S. Rauegi and W. J. Shaw, *Biochimica et biophysica acta*, 2014, **1837**, 131–138.
- 2756
- 2757 222 H. Long, P. W. King and C. H. Chang, *The journal of physical chemistry. B*, 2014, **118**, 890–900.
- 2758
- 2759 223 M. McCullagh and G. A. Voth, *The journal of physical chemistry. B*, 2013, **117**, 4062–4071.
- 2760
- 2761 224 A. J. Cornish, K. Gärtner, H. Yang, J. W. Peters and E. L. Hegg, *The Journal of biological chemistry*, 2011, **286**, 38341–38347.
- 2762
- 2763 225 P. Knörzer, A. Silakov, C. E. Foster, F. A. Armstrong, W. Lubitz and T. Happe, *The Journal of biological chemistry*, 2012, **287**, 1489–1499.
- 2764
- 2765 226 S. Morra, A. Giraudo, G. Di Nardo, P. W. King, G. Gilardi and F. Valetti, *PLoS one*, 2012, **7**, e48400.
- 2766
- 2767 227 E. Garcin, X. Venede, E. C. Hatchikian, A. Volbeda, M. Frey and J. C. Fontecilla-Camps, *Structure (London, England : 1993)*, 1999, **7**, 557–566.
- 2768
- 2769 228 A. Volbeda, P. Amara, C. Darnault, J.-M. M. Mouesca, A. Parkin, M. M. Roessler, F. A. Armstrong and J. C. Fontecilla-Camps, *Proceedings of the National Academy of Sciences of the United States of America*, 2012, **109**, 5305–5310.
- 2770
- 2771 229 I. Sumner and G. A. Voth, *The journal of physical chemistry. B*, 2012, **116**, 2917–2926.
- 2772
- 2773 230 E. Szőri-Dorogházi, G. Maróti, M. Szőri, A. Nyilasi, G. Rákhely and K. L. Kovács, *PLoS one*, 2012, **7**, e34666+.
- 2774
- 2775 231 S. Dementin, B. Burlat, A. L. De Lacey, A. Pardo, G. Adryanczyk-Perrier, B. Guigliarelli, V. M. Fernandez and M. Rousset, *The Journal of biological chemistry*, 2004, **279**, 10508–10513.
- 2776
- 2777 232 A. Gebler, T. Burgdorf, A. L. De Lacey, O. Rüdiger, A. Martinez-Arias, O. Lenz and B. Friedrich, *The FEBS journal*, 2007, **274**, 74–85.
- 2778
- 2779 233 R. Cammack, M. Frey and R. Robson, (editors) *Hydrogen as a fuel, learning from Nature*, Taylor and Francis, London and New York, 2001.
- 2780
- 2781 234 K. L. Pankhurst, C. G. Mowat, E. L. Rothery, J. M. Hudson, A. K. Jones, C. S. Miles, M. D. Walkinshaw, F. A. Armstrong, G. A. Reid and S. K. Chapman, *The Journal of biological chemistry*, 2006, **281**, 20589–20597.
- 2782
- 2783 235 C. M. Maupin, R. McKenna, D. N. Silverman and G. A. Voth, *J. Am. Chem. Soc.*, 2009, **131**, 7598–7608.
- 2784
- 2785 236 C. N. Schutz and A. Warshel, *J. Phys. Chem. B*, 2004, **108**, 2066–2075.
- 2786
- 2787
- 2788
- 2789
- 2790
- 2791
- 2792
- 2793

